Boundary feedback control of an anti-stable wave equation

Pierre Apkarian, Dominikus Noll

BOUNDARY FEEDBACK CONTROL OF AN ANTI-STABLE WAVE EQUATION

PIERRE APKARIAN[1] AND DOMINIKUS NOLL[2]

Abstract. We discuss boundary control of a wave equation with a non-linear anti-damping boundary condition. We design structured finite-dimensional H_∞-output feedback controllers which stabilize the infinite dimensional system exponentially in closed loop. The method is applied to control torsional vibrations in drilling systems with the goal to avoid slip-stick.

Key words: Wave equation · boundary feedback control · anti-damping boundary · infinite-dimensional H_∞-control · slip-stick · torsional vibrations · large magnitude sector non-linearity

1. Introduction

We discuss H_∞-boundary feedback control of a wave equation with instability caused by boundary anti-damping. This is applied to the control of vibrations in drilling devices. The system we consider is of the form

$$G_{nl}: \quad \begin{aligned} x_{tt}(\xi,t) &= x_{\xi\xi}(\xi,t) - 2\lambda x_t(\xi,t) \qquad 0<\xi<1, t\geq 0 \\ x_\xi(1,t) &= -x_t(1,t) + u(t) \\ \alpha x_{tt}(0,t) &= x_\xi(0,t) + q x_t(0,t) + \psi\left(x_t(0,t)\right) \end{aligned} \tag{1}$$

where (x, x_t) is the state, $u(t)$ the control, and where the measured outputs are

$$y_1(t) = x_t(0,t), \quad y_2(t) = x_t(1,t). \tag{2}$$

The non-linearity ψ satisfies $\psi(0) = 0$, $\psi'(0) = 0$, and the steady state is $(x, x_t, u) = (0, 0, 0)$. The linearized system G is obtained from (1) by dropping the term $\psi(x_t(0,t))$.

The parameters satisfy $\lambda \geq 0$, $\alpha \geq 0$, while q is signed. System (1) was first discussed in [47, 18, 48] in the context of oil-well drilling. The author of [18] proves open-loop stability of (1) for the case $q < 0$ using Lyapunov's direct method. Since applications typically lead to the opposite case $q > 0$, where instability occurs, various control strategies have been proposed for that setting.

Lyapunov's direct method is used in [39, 40, 12, 13]. This either leads to infinite dimensional controllers, which in order to be implemented require subsequent discretization and controller order reduction, or to infinite dimensional observer-based controllers, where the PDE is built into the observer.

Delay system techniques are used in [38, 39, 41, 21, 4], but require $\lambda = 0$, which leads to an oversimplified model. Input shaping is used in [32], but as presented, also requires the un-damped model $\lambda = 0$. In [24] the cases $\alpha = 0$, $\lambda = 0$ and $\alpha = 0$, $\lambda > 0$ are discussed, respectively, via difference equations and Lyapunov's method.

Backstepping control is used in [44, 33, 17, 34, 35, 23], but with the exception of [17], where $\lambda = \alpha = 0$, leads to infinite dimensional or state feedback controllers, to which one will again have to add observers and apply discretization or system reduction to make them implementable. Infinite dimensional controllers can also be obtained with the

[1]ONERA, Department of System Dynamics, Toulouse, France.
[2]Institut de Mathématiques, Université de Toulouse, France.

method in [11]. Other ideas to avoid slip-stick include the design of feedforward startup trajectories [1], or manipulation of the weight on bit in [38, 39]. Model (1), (2) has also been used to control axial vibrations, see [39, 14], and for robotic drilling [14].

What these approaches have in common is that they are guided by the *method of proof* of infinite-dimensional stability. This leads to control laws with large state dimension which, in our opinion, are inconvenient to implement, and certainly not favored by practitioners. In contrast, approaches guided by *practical considerations* have also been applied to oil-well drilling [42, 15], but those use finite-dimensional approximate models. This makes it desirable to bridge between both approaches by designing practical controllers using the infinite-dimensional model (1). In the present work we design H_∞-controllers (cf. [52, 6, 5]) with the following requirements:

(a) The controller is output feedback and of a simple, implementable structure, like a reduced-order controller or a PID.
(b) The controller stabilizes the infinite-dimensional system (and not just a finite-dimensional approximation of it).
(c) H_∞-optimality of the controller is certified in closed loop with the infinite-dimensional system (and not just with a finite-dimensional approximation).
(d) Due to the achieved infinite-dimensional H_∞-performance, slip-stick is avoided, or at least mitigated.

These requirements are achieved by going through the steps of the following general H_∞-control scheme, which we proposed for boundary and distributed control of PDEs in [9, 5, 4], where it has already been applied successfully to a variety of applications.

Algorithm 1. Infinite-dimensional H_∞-design

▷ **Step 1** (`Steady-state`)**.** Compute steady state of non-linear system $G_{\rm nl}$ and obtain linearization G. Compute transfer function $G(s)$ and determine number n_p of unstable poles of G.

▷ **Step 2** (`Stabilize`)**.** Fix practical controller structure $K(\mathbf{x})$, and compute initial stabilizing controller $K(\mathbf{x}^0)$ for G. Use Nyquist test to certify stability of linear infinite-dimensional closed loop.

▷ **Step 3** (`Performance`)**.** Determine plant P with H_∞-performance and robustness specifications, addressing in particular the non-linearity.

▷ **Step 4** (`Optimize`)**.** Solve discretized infinite-dimensional multi-objective H_∞-optimization program using a non-smooth trust region or bundle method [5, 9].

▷ **Step 5** (`Certificate`)**.** Certify final result in infinite-dimensional system within pre-specified tolerance level as in [5, 9].

While some of the elements of algorithm 1 are standard, others need to be adapted to the current case and explained in detail. In section 2, the mechanical model for control $G_{\rm nl}$ will be derived. Its linearization G, transfer function, and open-loop properties will be discussed in sections 3 and 4. Locally exponentially stabilizing controllers will be synthesized in section 5, and H_∞-synthesis for the full, non-linear model in section 6 will complete the procedure. Numerical results are regrouped in section 7.

2. Model of drilling system

We derive model (1) from the setup of an oil-well drilling system, shown schematically in Fig. 1. The state of the system is described by the angular position $\theta(\xi,t)$ and angular speed $\theta_t(\xi,t)$ of the drillstring, where position $\xi=0$ refers to the rotary table (top), while

$\xi = L$ represents the drill bit (bottom hole assembly), with L the length of the string. The dynamic equation and boundary conditions are

$$
\begin{aligned}
GJ\theta_{\xi\xi}(\xi,t) &= I\theta_{tt}(\xi,t) + \beta\theta_t(\xi,t) \quad 0 < \xi < L, t \geq 0 \\
I_B\theta_{tt}(L,t) &= -GJ\theta_\xi(L,t) - \phi\left(\theta_t(L,t)\right) \\
\theta_t(0,t) &= \frac{GJ}{c_a}\theta_\xi(0,t) + \Omega(t)
\end{aligned} \tag{3}
$$

where G is the angular shear modulus, J is the geometrical moment of inertia, I is the inertia of the string, I_B is the lumped inertia of the bottom hole assembly, c_a is related to the local torsion of the drillstring, $\Omega(t)$ is the time-dependent rotational velocity coming from the rotary table at the top, used to drive and control the system, while the undriven bottom extremity (bit) is subject to a torque $\phi(\theta_t)$ representing rock-bit and mud-bit interaction of the drill bit, depending non-linearly on the rotary speed $\theta_t(L,t)$ at the bottom; [18, 46, 47, 48]. The torsional excitations of the drillstring caused by the frictional force $\phi(\theta_t(L,t))$ lead to twisting of the string, and this effect propagates along the structure from bit to top as a wave with damping factor $\beta > 0$. Similarly, alterations in the rotary speed $\Omega(t)$ at the top are transmitted to bottom by the same damped wave. This implies that a control action at the top will be delayed by one period of the wave before taking effect at the bottom. If measurements are taken only at the top, then the delay before a control action takes effect is even two periods.

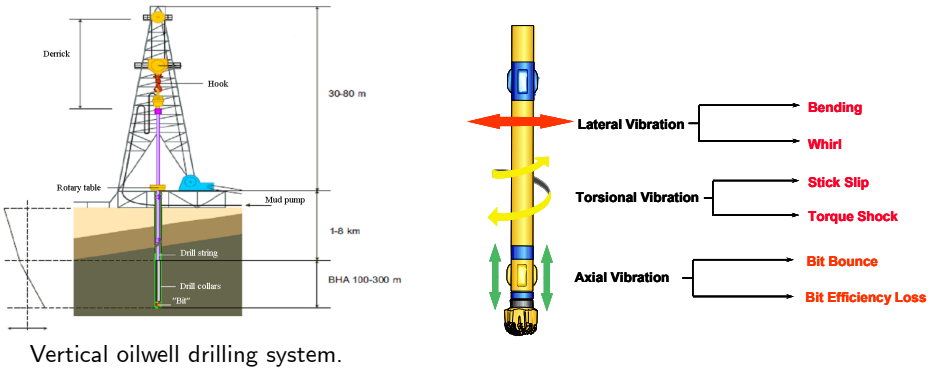

Vertical oilwell drilling system.

FIGURE 1.

The goal of the active control scenario is to maintain the system at steady state with constant rotational velocity $\theta_t(L,t) = \Omega$ at the drill bit position $\xi = L$ by acting on the driving rotary force $\Omega(t)$, and using measurements of the rotary speed at top and bottom. The steady state solution of (3) is easily obtained as

$$
\theta^0(\xi,t) = \Omega t - \left(\frac{\phi(\Omega) + \beta\Omega L}{GJ}\right)\xi + \frac{\beta\Omega}{2GJ}\xi^2
$$

and this corresponds to applying a constant control torque $\Omega(t) = \Omega_0$ at the top, where

$$
\Omega_0 = \Omega + \frac{\phi(\Omega) + \beta\Omega L}{c_a}.
$$

Writing the state in the form $\theta(\xi,t)=\theta^0(\xi,t)+\vartheta(\xi,t)$ for an off-set variable $\vartheta(\xi,t)$, and subtracting the steady state from (3), we obtain the equivalent system

$$\begin{aligned} GJ\vartheta_{\xi\xi}(\xi,t) &= I\vartheta_{tt}(\xi,t)+\beta\vartheta_t(\xi,t)\\ I_B\vartheta_{tt}(L,t) &= -GJ\vartheta_{\xi}(L,t)+\phi(\Omega)-\phi\left(\Omega+\vartheta_t(L,t)\right)\\ GJ\vartheta_{\xi}(0,t) &= c_a\left(\vartheta_t(0,t)-\Omega(t)+\Omega_0\right)\end{aligned} \tag{4}$$

A dimensionless system is now obtained by the change of variables

$$\xi=L(1-\zeta)\quad \tau=\frac{1}{L}\sqrt{\frac{GJ}{I}}t.$$

On putting $x(\zeta,\tau)=\vartheta(\xi,t)$, this leads to the following equivalent dimensionless form

$$\begin{aligned} x_{\zeta\zeta}(\zeta,\tau) &= x_{\tau\tau}(\zeta,\tau)+\frac{\beta L}{\sqrt{GJI}}x_\tau(\zeta,\tau)\\ \frac{I_B}{LI}x_{\tau\tau}(0,\tau) &= x_\zeta(0,\tau)+\frac{L}{GJ}\left(\phi(\Omega)-\phi\left(\Omega+\frac{1}{L}\sqrt{\frac{GJ}{I}}x_\tau(0,\tau)\right)\right)\\ x_\zeta(1,\tau) &= -\frac{c_a}{\sqrt{GJI}}x_\tau(1,\tau)+\frac{c_aL}{GJ}\left(\Omega(t)-\Omega_0\right)\end{aligned} \tag{5}$$

We re-write the second boundary condition of (5) at $\zeta=1$ as

$$x_\zeta(1,\tau)+x_\tau(1,\tau)=\left(1-\frac{c_a}{\sqrt{GJI}}\right)x_\tau(1,\tau)+\frac{c_aL}{GJ}\left(\Omega(\tau)-\Omega_0\right).$$

Taking into consideration that the measured outputs of (3) are the angular velocities at the top and bottom positions $y_1(t)=\theta_t(L,t)$, $y_2(t)=\theta_t(0,t)$, the outputs of the centered system (5) may be understood as measurements of the offset angular velocities $y_1(\tau)=x_\tau(0,\tau)$ and $y_2(\tau)=x_\tau(1,\tau)$. This allows us to introduce the control

$$u(\tau)=\left(1-\frac{c_a}{\sqrt{GJI}}\right)x_\tau(1,\tau)+\frac{c_aL}{GJ}\left(\Omega(\tau)-\Omega_0\right),$$

which when chosen in feedback form $u(\tau)=K(y_1(\tau),y_2(\tau))$ leads to the following final feedback control law for (3):

$$\Omega(t)=\Omega_0+\left[K(y_1(t),y_2(t))+\left(\frac{c_a}{\sqrt{GJI}}-1\right)y_2(t)\right]\frac{GJ}{c_aL},$$

which is linear as soon as $u=Ky$ is a linear controller. With that the second boundary condition takes indeed the form $x_\zeta(1,\tau)+x_\tau(1,\tau)=u(\tau)$ in (1).

Switching back for convenience to t for time and $\xi\in[0,1]$ for the spatial variable, and introducing the dimension free parameters

$$\alpha=\frac{I_B}{LI},\quad \lambda=\frac{\beta L}{2\sqrt{GJI}},\quad q=-\frac{\phi'(\Omega)}{\sqrt{GJI}}, \tag{6}$$

system (5) turns into the form (1) with the non-linearity given by

$$\psi(\omega)=\frac{L}{GJ}\left(\phi(\Omega)-\phi\left(\Omega+\frac{1}{L}\sqrt{\frac{GJ}{I}}\omega\right)\right)-q\cdot\omega, \tag{7}$$

and with

$$\psi'(\omega)=-\frac{\phi'\left(\Omega+\frac{1}{L}\sqrt{\frac{GJ}{I}}\omega\right)}{\sqrt{GJI}}-q,\quad \psi''(\omega)=-\frac{\phi''\left(\Omega+\frac{1}{L}\sqrt{\frac{GJ}{I}}\omega\right)}{LI}.$$

From the definition of q it can be readily seen that $\psi(0) = 0$ and $\psi'(0) = 0$, which complies with the requirement in (1). For later use, we introduce an additional parameter

$$p := \psi''(0),$$

which represents the curvature of the non-linearity at the reference position, and gives information on its severity.

FIGURE 2. The case $\phi'(\Omega) > 0$ (left) leads to a stable open loop [18]. The potentially unstable case (right) is when increasing rotary speed reduces friction.

Phenomenological models of the frictional force $\phi(\cdot)$ have been proposed in the literature. For instance [27] considers a model of the form

$$\phi(\theta_t) = \phi_{\text{mud}}(\theta_t) + \phi_{\text{rock}}(\theta_t),$$

where the mud friction is assumed of viscous form $\phi_{\text{mud}}(\theta_t) = c_b \cdot \theta_t$, while the rock-bit interaction is the non-linear

$$\phi_{\text{rock}}(\theta_t) = W_{ob} R_b \left[\mu_{cb} + (\mu_{sb} - \mu_{cb})\, e^{-\frac{\gamma_b}{\nu_f}|\theta_t|}\right] \text{sign}(\theta_t), \qquad \phi_{\text{mud}}(\theta_t) = c_b \cdot \theta_t. \tag{8}$$

Here W_{ob} is the weight on bit, R_b is the radius of the drill, the non-linear term features the static and Coulomb friction coefficients $\mu_{sb}, \mu_{cb} \in (0, 1)$, while the coefficient $\gamma_b \in (0, 1)$ is the velocity decrease rate accounting for the Stribeck effect. The fact that $\mu_{sb} > \mu_{cb}$ is the ultimate reason why the slip-stick phenomenon may occur. Namely, for $\Omega > 0$ we have $\phi'(\Omega) = c_b - W_{ob} R_b (\gamma_b/\nu_f)\, (\mu_{sb} - \mu_{cb})\, e^{-(\gamma_b/\nu_f)\Omega}$, which leads to

$$q = \frac{-c_b + W_{ob} R_b (\gamma_b/\nu_f)\, (\mu_{sb} - \mu_{cb})\, e^{-(\gamma_b/\nu_f)\Omega}}{\sqrt{GJI}}$$

which is typically positive due to dominance of the rock-bit over the mud-bit interaction. In contrast, the curvature parameter

$$p = \psi''(0) = -\frac{1}{LI}\phi''(\Omega) = -\frac{W_{ob} R_b\, (\mu_{sb} - \mu_{cb})\, (\gamma_b/\nu_f)^2 e^{-(\gamma_b/\nu_f)\Omega}}{LI}$$

is typically negative.

3. Analysis of the linear system G

In this section we determine the number of unstable poles of the linearization G of G_{nl}, as this will be needed later to assure stability of the closed loop. This discussion is of independent interest, as in a different context the specific form of the non-linearity $\psi(x_t)$ may be unknown, in which case a linear parametric robust synthesis in q may be required.

We recall from [18] that the open loop G_{nl} is stable for $\phi' > 0$, and the same is true for its linearization G. This means that we may concentrate on the potentially instable case $\phi' \leq 0$, which means $q \geq 0$. Our goal is to classify the open loop properties of G as a function of the three parameters $(q, \alpha, \lambda) \in \mathbb{R}^3_+$.

Five scenarios of physical parameters

	gray	blue	magenta	red	green	
G	79.3e9	79.3e9	79.3e9	79.3e9	79.3e9	$\mathrm{N}\cdot\mathrm{m}^{-2}$
J	1.19e-5	1.19e-5	1.19e-5	1.19e-5	1.19e-5	m^4
I	0.095	0.095	0.095	0.095	0.095	$\mathrm{kg}\cdot\mathrm{m}$
I_B	89	35.6	35.6	35.6	89	$\mathrm{kg}\cdot\mathrm{m}^2$
L	1172	2050	1172	2050	1172	m
Ω	10	10	10	10	10	$\mathrm{rad}\cdot\mathrm{s}^{-1}$
c_a	2000	2000	2000	2000	2000	$\mathrm{kg}\cdot\mathrm{m}^2\cdot\mathrm{s}^{-1}$
β	0.1	0.16	0.01 / 0.5	0.01/0.1	0.02	$\mathrm{N}\cdot\mathrm{s}$
W_{ob}	97347	146020.5	146020.5	146020.5	146020.5	N
R_b	0.155575	0.18202275	0.2022475	0.2333625	0.2022475	m
μ_{sb}	0.8	0.8	0.8	0.8	0.8	rad
μ_{cb}	0.5	0.5	0.5	0.5	0.5	rad
γ_b	0.9	0.1	0.1	0.1	0.1	–
ν_f	1	1	1	1	1	$\mathrm{rad}\cdot\mathrm{s}^{-1}$
c_b	0.03	0.03	0.03	0.03	0.03	N m s

TABLE 1

Derived parameters of five scenarios

	gray	blue	magenta	red	green	
Ω_0	15.02	19.75	21.94	20.50	19.13	$\mathrm{rad}\cdot\mathrm{s}^{-1}$
$-\frac{\Omega L\sqrt{I}}{\sqrt{GJ}}$	-3.7186	-6.5044	-3.7186	-6.5044	-3.7186	rad
λ	0.1957	0.5477	0.9786	0.03423	0.0391	–
α	0.7994	0.1828	0.3197	0.1828	0.7994	–
q	0.0019	0.9796	1.0885	1.2559	1.0885	–
p	-0.0048	-0.1506	-0.2927	-0.1931	-0.2927	–
τ/t	2.6892	1.5374	2.6892	1.5374	2.6892	s^{-1}
n_p	0	2	2	1	1	
n_z	0	4	2	22	4	

TABLE 2

Laplace transformation of (1) leads to a family of one-dimensional boundary value problems parametrized by $s \in \mathbb{C}$:

$$G: \begin{aligned} x_{\xi\xi}(\xi,s) &= (s^2+2\lambda s)x(\xi,s) \\ x_\xi(1,s) &= -sx(1,s)+u(s) \\ x_\xi(0,s) &= (\alpha s^2 - qs)x(0,s) \end{aligned} \tag{9}$$

which we solve explicitly. With the outputs $y_1(s) = sx(0,s)$, $y_2(s) = sx(1,s)$ from (2) we obtain

(10)

$$G(s) = \begin{bmatrix} \frac{y_1(s)}{u(s)} \\ \\ \frac{y_2(s)}{u(s)} \end{bmatrix} = \begin{bmatrix} \frac{1}{\frac{e^\sigma - e^{-\sigma}}{2\sigma}\left[\frac{\sigma^2}{s}+\alpha s^2 - qs\right] + \frac{e^\sigma+e^{-\sigma}}{2}\left[\alpha s - q + 1\right]} \\ \\ \frac{\frac{e^\sigma+e^{-\sigma}}{2} + (\alpha s^2 - qs)\frac{e^\sigma - e^{-\sigma}}{2\sigma}}{\frac{e^\sigma - e^{-\sigma}}{2\sigma}\left[\frac{\sigma^2}{s}+\alpha s^2 - qs\right] + \frac{e^\sigma+e^{-\sigma}}{2}\left[\alpha s - q + 1\right]} \end{bmatrix}, \quad \sigma(s) := \sqrt{s^2+2\lambda s}.$$

We now have to determine the number of unstable poles of (10) as a function of $(q,\alpha,\lambda) \in \mathbb{R}^3_+$. Note that $G(s) = [1/d(s), n(s)/d(s)]^T$ is a meromorphic function, with $n(s), d(s)$ in

(10) holomorphic, but its analysis is more complicated than that of a pure delay system due to the damping coefficient λ and the consequent appearance of the term $\sigma(s)$.

Annihilating $d(s) = (s + 2\lambda + \alpha s^2 - qs)\frac{e^\sigma - e^{-\sigma}}{2\sigma} + (\alpha s - q + 1)\frac{e^\sigma + e^{-\sigma}}{2} = 0$ leads to the complex equation

$$q - \alpha s - 1 = \frac{2\lambda}{s + \frac{(e^\sigma + e^{-\sigma})/2}{(e^\sigma - e^{-\sigma})/2\sigma}} =: \Phi(\lambda, s), \tag{11}$$

which relates unstable pole $s \in \overline{\mathbb{C}}_+ = \{s \in \mathbb{C} : \mathrm{Re}(s) \geq 0\}$ of $G(s)$ and damping coefficient $\lambda > 0$ to the pair (q, α) through the operator Φ. Since this is a complex equation and q, α are real, we deduce

$$\alpha = -\frac{\mathrm{Im}\,\Phi(\lambda, s)}{\mathrm{Im}(s)}, \quad q - 1 = \frac{\mathrm{Re}\,\Phi(\lambda, s)\mathrm{Im}(s) - \mathrm{Im}\,\Phi(\lambda, s)\mathrm{Re}(s)}{\mathrm{Im}(s)}. \tag{12}$$

We have proved the following

Lemma 1. *Let $\lambda > 0$ and $s \in \overline{\mathbb{C}}_+$. Suppose (q, α) given by (12) is in $\mathbb{R}^2_+$. Then s is an unstable pole of G for the parameters $(q, \alpha, \lambda) \in \mathbb{R}^3_+$.* □

Let us look at poles on the imaginary axis $j\mathbb{R}$, referred to as *zero-crossings*. Going back to (11) with $s = j\omega$ gives

Lemma 2. *Let $\lambda > 0$ and $\omega \in \mathbb{R}$. Suppose the pair*

$$q - 1 = \mathrm{Re}\,\Phi(\lambda, j\omega), \quad \alpha = -\frac{\mathrm{Im}\,\Phi(\lambda, j\omega)}{\omega}$$

satisfies $(q, \alpha) \in \mathbb{R}^2_+$. Then $j\omega$ is a zero crossing (unstable pole on $j\mathbb{R}$) of G for the parameter $(q, \alpha, \lambda) \in \mathbb{R}^3_+$. □

Let us look more specifically at zero-crossings through the origin. Substituting $s = 0$ in the denominator $d(s)$ in (10) and equating $d(0) = 0$ gives the relation

$$q - 1 = 2\lambda_{\mathrm{crit}}$$

which says that for $q > 1$ a real pole of G crosses the imaginary axis through the origin at the critical value $\lambda = \lambda_{\mathrm{crit}}$. Here we use the fact that $\Phi(\lambda, 0) = 2\lambda$, explained by the relations

$$\frac{e^\sigma - e^{-\sigma}}{2\sigma} = 1 + \frac{\sigma^2}{3!} + \frac{\sigma^4}{5!} + \ldots, \frac{e^\sigma + e^{-\sigma}}{2} = 1 + \frac{\sigma^2}{2!} + \frac{\sigma^4}{4!} + \ldots, \frac{\sigma^2}{s} = s + 2\lambda. \tag{13}$$

Theorem 1. *For fixed $(q, \alpha, \lambda) \in \mathbb{R}^3_+$ there exists $R > 0$ such that G has no poles and no transmission zeros on $\{s \in \overline{\mathbb{C}}_+ : |s| \geq R\}$.*

Proof: 1) For unstable poles we have to show that equation (11), respectively, (12) has no solutions when $s \in \overline{\mathbb{C}}_+$ and $|s| \gg 0$ sufficiently large. Let $s = \mu + j\omega$, $\sigma = a + jb$, then by the definition of σ:

$$a^2 - b^2 = \mu^2 - \omega^2 + 2\lambda\mu, \quad ab = \omega(\mu + \lambda). \tag{14}$$

It follows that for fixed $a_0 > 0$ the set $\{s \in \overline{\mathbb{C}}_+ : \mathrm{Re}(\sigma) \leq a_0\}$ is bounded. Choose $R_1 > 0$ such that $\{s \in \overline{\mathbb{C}}_+ : \mathrm{Re}(\sigma) \leq a_0\} \subset \{s \in \overline{\mathbb{C}}_+ : |s| \leq R_1\}$. It remains to discuss candidate poles $s \in \overline{\mathbb{C}}_+$ with $\mathrm{Re}(\sigma) \geq a_0$ for some fixed $a_0 > 0$.

2) Consider $s \in \overline{\mathbb{C}}_+$ with $\mathrm{Re}(\sigma) = a \geq a_0$ and define

$$\theta := \frac{e^\sigma + e^{-\sigma}}{e^\sigma - e^{-\sigma}} = \frac{1 + e^{-2a}e^{-j2b}}{1 - e^{-2a}e^{-j2b}}.$$

Then $\frac{1+\rho_0}{1-\rho_0} \geq |\theta| \geq \frac{1-\rho_0}{1+\rho_0}$, where $\rho_0 = e^{-2a_0}$. Moreover, we have $|\theta + 1| \geq \frac{2}{1+e^{-2a_0}} =: \theta_0 > 1$. Now choose $\epsilon > 0$ such that $\frac{1+\rho_0}{1-\rho_0}\,\epsilon < \theta_0/2$. Since λ is fixed we have $\sigma/s \to 1$ as $s \to \infty$

on $\mathbb{C}^+$, hence there exists $M = M(\lambda) > 0$ such that $|s - \sigma| < \epsilon|s|$ for all $|s| \geq M$. Then $|s + \theta\sigma| = |\theta(\sigma - s) + (\theta + 1)s| \geq |\theta + 1||s| - |\theta||s - \sigma| \geq \theta_0|s| - |\theta|\epsilon|s| \geq \theta_0|s|/2$ for $|s| \geq M$. Writing (11) as

$$q - 1 - \alpha s = \Phi(\lambda, s) = \frac{2\lambda}{s + \theta\sigma}, \tag{15}$$

and taking into account that on the right hand side we now have

$$|\Phi(\lambda, s)| = \frac{2\lambda}{|s + \theta\sigma|} \leq \frac{4\lambda}{\theta_0|s|},$$

we see that (15) can have no solution for $|s| \geq \max\{\frac{4\lambda}{\alpha\theta_0}, 1 + \frac{1+q}{\alpha}, M, R_1\} =: R$. That settles the case $\alpha > 0$.

3) For $\alpha = 0$ and $q \neq 1$ there are no poles in $|s| > \frac{4\lambda}{|q-1|\theta_0}$, and for $q = 1$, $\alpha = 0$ clearly (15) has no solutions.

4) Let us next discuss unstable zeros. Clearly those can only occur in the second component y_2/u in (10). Here the equation is $\Phi(\lambda, s)^{-1} = \frac{(q+1)s - \alpha s^2}{2\lambda}$. From 1) above we know that we may concentrate on $\mathrm{Re}(\sigma) \geq a_0$, and from 2) we have $|\theta| \leq \frac{1+\rho_0}{1-\rho_0}$, while for $|s| > \lambda$ we get $|\sigma| \leq \sqrt{3}|s|$, hence for $|s| > \max\{R_1, \lambda\}$:

$$|\Phi(\lambda, s)| = \left|\frac{2\lambda}{s + \theta\sigma}\right| \geq \frac{2\lambda}{|s| + |\theta||\sigma|} \geq \frac{2\lambda}{|s|(1 + \frac{1+\rho_0}{1-\rho_0}\sqrt{3})}.$$

This leads to

$$\frac{|(q+1)s - \alpha s^2|}{2\lambda} = |\Phi(\lambda, s)|^{-1} \leq \frac{|s|(1 + \frac{1+\rho_0}{1-\rho_0}\sqrt{3})}{2\lambda},$$

hence

$$\alpha|s| - (q+1) \leq |\alpha s - (q+1)| \leq 1 + \frac{1+\rho_0}{1-\rho_0}\sqrt{3}.$$

For $\alpha > 0$ this cannot be satisfied for large $|s|$. In fact, there are no unstable zeros on $|s| > R := \max\{R_1, \lambda, (2 + q + \frac{1+\rho_0}{1-\rho_0}\sqrt{3})/\alpha\}$. For $\alpha = 0$ the equation for unstable zeros is $\theta\sigma = qs$, and since $\sigma/s = \sqrt{1 + 2\lambda/s} \to 1$ for $s \to \infty$, we get $\theta \to q$. On choosing a_0 sufficiently large, we get $\theta \approx 1$, which leads to a contradiction for $q \neq 1$. Finally, for $q = 1, \alpha = 0$ we obtain the transfer function $y_2/u = \frac{s[(\sigma-s)e^{\sigma} + (\sigma+s)e^{-\sigma}]}{(\sigma-s)(\sigma+s)e^{\sigma} - (\sigma+s)^2e^{-\sigma}}$, so unstable zeros $\neq 0$ satisfy $\frac{s-\sigma}{s+\sigma} = e^{-2\sigma}$. That gives $-\frac{\lambda}{s+\sigma+\lambda} = e^{-2\sigma}$, which cannot be satisfied for large $|s|$. □

Since the transfer function G is of size 2×1, the number of unstable poles is the maximum of the number of unstable poles of $G_1(s) = 1/d(s)$ and $G_2(s) = n(s)/d(s)$, hence the number of unstable zeros of $d(s)$. The latter can be determined by the argument principle. For the following we denote the half circle used for the standard Nyquist contour by D_R.

Proposition 1. *Suppose $(q, \alpha, \lambda) \in \mathbb{R}^3_+$ does not give rise to zero crossings. Then the number n_p of unstable poles of $G(s)$ equals the winding number of $d(\mathsf{D}_R)$ around 0, where the radius $R > 0$ is as in Theorem 1.*

The radius R in Theorem 1 may be quantified, and the winding number can be computed exactly using the method in [5]. If (q, α, λ) creates a zero-crossing, the contour D_R has to be modified, either by making small indentations into the right half plane, or preferably by removing poles on $j\mathbb{R}$ with the method of [25], as explained in [5]. At this stage we have completed step 1 of our general algorithm 1.

We conclude this section with the following important consequence of Theorem 1.

Corollary 1. *The input-output map and the input-to-state map of the boundary control problem* (1) *are bounded.*

Proof: As a consequence of [20, Thm. 2.3] for input-output boundedness it suffices to show that $\sup_{\mathrm{Re}(s)>a_0} |G_2(s)| < \infty$ for some $a_0 \in \mathbb{R}$. We choose a_0 as in the proof of Theorem 1, which allows us to bring θ as close to 1 as we wish. Now with the notation of the theorem

$$G_2(s) = \frac{\sigma\theta + \alpha s^2 - qs}{\sigma^2/s + \alpha s^2 - qs + 2\sigma\theta(\alpha s - q + 1)}.$$

For $\alpha > 0$ we divide numerator and denominator by the leading term αs^2, which gives

$$G_2(s) = \frac{1 + \sigma\theta/\alpha s^2 - q/\alpha s}{1 + 1/\alpha s + 2\lambda/\alpha s^2 - q/\alpha s + 2\theta\sigma/s + 2(1-q)\sigma\theta/\alpha s^2} \sim \frac{1}{1 + 2\theta\sigma/s}.$$

But $\sigma^2/s^2 = 1 + 2\lambda/s \sim 1$, whence $G_2(s) \sim 1/3$, showing that G_2 is bounded on some half plane $\mathrm{Re}(s) > a_0$. Since $G_2 = n/d$ and $G_1 = 1/d$, this is also true for G_1. In the case $\alpha = 0$ simplification by s leads to a similar estimate. For the input-to-state map we repeat the argument with $G(\xi, s) = sx(\xi, s)/u(s)$. □

4. Pattern of unstable poles

As a consequence of the previous section we can determine the number n_p of unstable poles of G for every scenario $(q, \alpha, \lambda) \in \mathbb{R}^3_+$ using the argument principle. However, we would like to learn a little more about $n_p(q, \alpha, \lambda)$, and in this section we shall see that $n_p \in \{0, 1, 2\}$, where the corresponding regions can be determined with arbitrary numerical precision.

To begin with, observe that for $\lambda = 0$ the transfer function (due to $\sigma = s$) simplifies to a pure delay system

$$G_{\lambda=0}(s) = \begin{bmatrix} \dfrac{e^{-s}}{1 + \alpha s - q} \\ \dfrac{(1 + \alpha s - q) + (1 - \alpha s + q)e^{-2s}}{2(1 + \alpha s - q)} \end{bmatrix} = \begin{bmatrix} \dfrac{\frac{1}{\alpha}e^{-s}}{s - \frac{q-1}{\alpha}} \\ \dfrac{1}{2} + \dfrac{\frac{1}{2}\left(\frac{1+q}{\alpha} - s\right)e^{-2s}}{s - \frac{q-1}{\alpha}} \end{bmatrix},$$

where we immediately see that $G_{\lambda=0}$ has one unstable real pole if $q \geq 1$, while it is stable for $q < 1$.

This suggests now the following procedure. Fix $(q, \alpha) \in \mathbb{R}^2_+$, and then follow the evolution of the number of unstable poles $n_p(\lambda) := n_p(q, \alpha, \lambda)$ of G as λ increases from $\lambda = 0$ to $\lambda \to +\infty$. We know the number of poles at $\lambda = 0$, and we expect that for very large $\lambda > 0$ the damping effect in the wave equation should lead back to stability, $n_p(\lambda) = 0$ as $\lambda \to \infty$.

Let us look again at zero crossings at the origin. We know that for $q > 1$ the origin is crossed when $\lambda \in [0, \infty)$ reaches the critical value $\lambda_{\mathrm{crit}} = (q-1)/2 > 0$. We have to decide whether this real pole when crossing $s = 0$ migrates from left to right or in the opposite direction. Let $s(\lambda)$ be the position of the potentially unstable pole on the real axis, that is $d\,(s(\lambda), \lambda) = 0$, where $s(\lambda_{\mathrm{crit}}) = 0$. Writing $d(s, \lambda)$ for the denominator d in (10) to highlight dependency on both s, λ, we apply the implicit function theorem at $(s(\lambda_{\mathrm{crit}}), \lambda_{\mathrm{crit}}) = (0, \lambda_{\mathrm{crit}})$ under the hypothesis $d_s(0, \lambda_{\mathrm{crit}}) \neq 0$, which is equivalent to $\alpha \neq \frac{1}{3}(q-1)^2 + (q-1)$. Then differentiation with respect to λ gives

$$s'(\lambda) = -\frac{d_\lambda(s(\lambda), \lambda)}{d_s(s(\lambda), \lambda)},$$

where the partial derivatives with respect to λ, s are

$$d_\lambda = 2\left(1+\frac{\sigma^2}{3!}+\dots\right)+(s+2\lambda+\alpha s^2-qs)\frac{s}{\sigma}\left(\frac{2\sigma}{3!}+\frac{4\sigma^2}{5!}+\dots\right)+(\alpha s-q+1)\frac{s}{\sigma}\frac{e^\sigma+e^{-\sigma}}{2}$$

and

$$d_s = (1+2\alpha s-q)\left(1+\frac{\sigma^2}{3!}+\dots\right)+(s+2\lambda+\alpha s^2-qs)\frac{s+\lambda}{\sigma}\left(\frac{2\sigma}{3!}+\frac{4\sigma^3}{5!}+\dots\right)$$
$$+\alpha\frac{e^\sigma+e^{-\sigma}}{2}+(\alpha s-q+1)\frac{e^\sigma-e^{-\sigma}}{2\sigma}(s+\lambda).$$

Substituting $\lambda=\lambda_{\rm crit}=(q-1)/2$ and $s=s(\lambda_{\rm crit})=0$ gives

$$s'(\lambda_{\rm crit})=\frac{2}{\frac{1}{3}(q-1)^2+(q-1)-\alpha}.$$

Hence

$$s'(\lambda_{\rm crit})\begin{cases}>0 & \text{for } \alpha<\frac{1}{3}(q-1)^2+(q-1)\\ <0 & \text{for } \alpha>\frac{1}{3}(q-1)^2+(q-1)\end{cases}$$

This leads to the following

Lemma 3. *Let $(q,\alpha)\in\mathbb{R}^2_+$. If $\alpha<\frac{1}{3}(q-1)^2+(q-1)$, then a single real pole of G crosses the imaginary axis through the origin at $\lambda=\lambda_{\rm crit}=(q-1)/2$ from left to right, going from stable at $\lambda<\lambda_{\rm crit}$ to unstable at $\lambda_{\rm crit}<\lambda$. If $\alpha>\frac{1}{3}(q-1)^2+(q-1)$ a single real pole crosses the imaginary axis through the origin from right to left, going from unstable at $\lambda<\lambda_{\rm crit}$ to stable at $\lambda>\lambda_{\rm crit}$.* □

This can also be corroborated by investigating the value $G(0)$ in (10). We have

$$G_1(0)=\frac{1}{2\lambda-q+1},$$

so G has no unstable pole at the origin, except for the critical λ value $\lambda_{\rm crit}=(q-1)/2$ when $q>1$. On the exceptional manifold $\mathbb{M}=\{(q,\alpha,\lambda)\in\mathbb{R}^3_+ : 2\lambda=q-1\}$, we have

$$\lim_{s\to0} sG_1(s)=\frac{1}{\alpha-(q-1)-\frac{1}{3}(q-1)^2},$$

which means a pole of order one at the origin, except when (q,α) lies on the parabola $\alpha=(q-1)+\frac{1}{3}(q-1)^2$. On the exceptional set $\mathbb{O}=\{(q,\alpha,\lambda)\in\mathbb{R}^3_+ : 2\lambda=q-1, \alpha=(q-1)+\frac{1}{3}(q-1)^2\}$ we find that

$$\lim_{s\to0} s^2G_1(s)=\frac{6}{q^2-1},$$

which means G has a double pole at the origin, except when $q=1$. The case $q=1$ now leaves only the parameter choice $(q,\alpha,\lambda)=(1,0,0)$, an exceptional point where the system is not well-posed.

Using the mapping Φ, one can see that the positive quadrant $(q,\alpha)\in\mathbb{R}^2_+$ may be divided into 5 different zones, shown in Fig. 3, in which the number of unstable poles of G evolves differently. Each zone has its specific pattern.

The red zone is $\texttt{Red}=\{(q,\alpha) : q\ge1, \alpha\ge0, \alpha\le\frac{1}{3}(q-1)^2+(q-1)\}$ is below a parabola. Setting

$$m(q)=\sup\{\alpha>0 : q-1=\mathrm{Re}\,\Phi(\lambda,j\omega), \alpha=-\omega^{-1}\mathrm{Im}\,\Phi(\lambda,j\omega) \text{ for certain } \omega>0,\ \lambda>0\},$$

the magenta zone is defined as

$$\texttt{Mag}=\{(\alpha,q) : q\ge1, \tfrac{1}{3}(q-1)^2+(q-1)\le\alpha\le m(q)\}$$

delimited by the parabola and the analytic curve $\alpha = m(q)$. The green zone is

$$\texttt{Green} = \{(q,\alpha) : q \geq 1, \alpha \geq m(q)\},$$

where the curve $\alpha = m(q)$ separates magenta and green. Finally, on setting

$$b(\alpha) = \inf\{q : q - 1 = \operatorname{Re}\Phi(\lambda, j\omega), \alpha = -\omega^{-1}\operatorname{Im}\Phi(\lambda, j\omega) \text{ for certain } \omega > 0,\ \lambda > 0\},$$

the blue zone is $\texttt{Blue} = \{(q,\alpha) : \alpha \geq 0, b(\alpha) \leq q \leq 1\}$, which is the only bounded one. The boundary of the blue zone described by the curve $q = b(\alpha)$ is just a different local parametrization of the same analytic curve $\alpha = m(q)$ separating magenta and green. This curve disappears into $\alpha < 0$ at $(1,0)$, where it is no longer of interest. The gray zone `Gray` is what is left over from the strip $0 \leq q \leq 1$, $\alpha \geq 0$ when removing the blue zone.

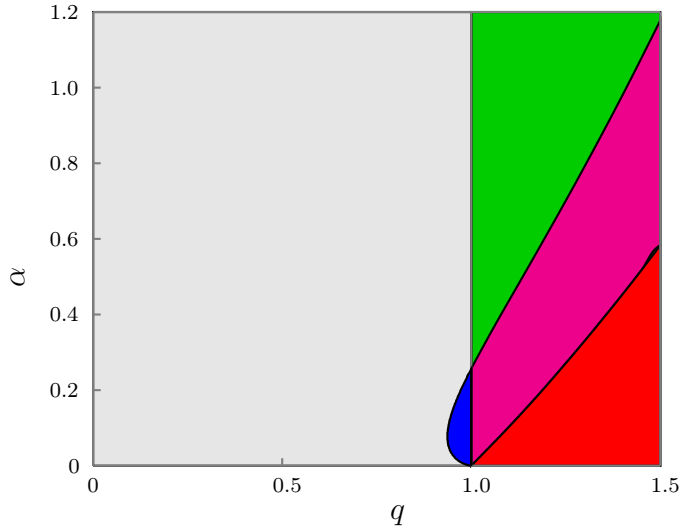

FIGURE 3. Five regions and five scenarios. The pattern of the gray zone is 0. Blue: 0-2-0. Red: 1-2-0. Magenta: 1-0-2-0. Green: 1-0.

Altogether, we have found the following classification or pattern.

- For $(q,\alpha) \in \texttt{Gray}$ the system G is stable for all $\lambda \geq 0$. The pattern is `0`.
- For $(q,\alpha) \in \texttt{Blue}$ there exist $0 < \lambda_1(q,\alpha) < \lambda_2(q,\alpha)$ such that G is stable for all $0 \leq \lambda < \lambda_1(q,\alpha)$ and $\lambda > \lambda_2(q,\alpha)$, and has two unstable poles for $\lambda_1 \leq \lambda \leq \lambda_2$. The pattern is `0-2-0`.
- For $(q,\alpha) \in \texttt{Red}$ the system has one unstable pole for $0 \leq \lambda \leq (q-1)/2 =: \lambda_1(q)$, and two unstable poles for $(q-1)/2 \leq \lambda \leq \lambda_2(q,\alpha)$, while it is again stable for $\lambda > \lambda_2(q,\alpha)$. The pattern is `1-2-0`.
- For $(q,\alpha) \in \texttt{Mag}$ there exist $\lambda_2(q,\alpha) > \lambda_1(q,\alpha) > (q-1)/2$ such that the system has one unstable pole for $0 \leq \lambda \leq (q-1)/2$, no unstable poles for $(q-1)/2 < \lambda < \lambda_1(q,\alpha)$, then two unstable poles for $\lambda_1(q,\alpha) \leq \lambda \leq \lambda_2(q,\alpha)$, and again no unstable poles for $\lambda > \lambda_2(q,\alpha)$. The pattern is `1-0-2-0`.
- For $(q,\alpha) \in \texttt{Green}$ the system has one unstable pole for $0 \leq \lambda \leq (q-1)/2$, and is stable for $\lambda > (q-1)/2$. The pattern is `1-0`.

Remark 1. The values $\lambda_1(\alpha, q)$, $\lambda_2(\alpha, q)$ for each zone can be computed with arbitrary precision. We mention that [24] discusses among others the case $\alpha = 0, \lambda > 0$ and finds sufficient conditions on $q > 0$ for open loop stability. This is corroborated by our findings, because $(0, q) \in \texttt{Gray}$ for $0 < q < 1$.

5. Stabilization

In this section we pave the way to construct finite-dimensional output feedback controllers which stabilize the linearization G of system (1)–(2) exponentially. The following result is preparatory, as it allows to upgrade H_∞-stability of the closed loop into exponential stability. The idea of the proof is the following. According to [26, Theorem 5.2], a well-posed system which is exponentially stabilizable, exponentially detectable, and at the same time H_∞-stable, is already exponentially stable in the state-space sense. In order to apply this result to the closed-loop system, several transformations of the original state-space are performed.

Theorem 2. *Let K be a finite-dimensional output feedback controller for (1)-(2) which stabilizes the linearized system G in the H_∞-sense. Then the linearized closed loop (G, K) is even exponentially stable.*

Proof: 1) We start with a preparatory argument. Suppose the boundary control problem is written in the abstract form

$$\dot{x} = \mathscr{A}x, \quad \mathscr{P}x = u, \quad y = \mathscr{C}x \tag{16}$$

with suitable unbounded operators [20, 36, 37], and the controller $u = Ky$ stabilizes (16) in the H_∞-sense. Writing $K(s) = K_1(s) + K_0$ with K_1 strictly proper, we see that $\widetilde{u} = K_1 y$ stabilizes the modified boundary control problem

$$\dot{x} = \mathscr{A}x, \quad (\mathscr{P} - K_0\mathscr{C})x = \widetilde{u}, \quad y = \mathscr{C}x$$

in the H_∞-sense, where $\widetilde{u} = u - K_0 y$. We will use this type of shift in part 3) below to arrange for a strictly proper stabilizing controller.

2) Starting out from the linearization G of (1) we perform the change of variables $z(\xi, t) = x_\xi(\xi, t)$, $v(t) = x_t(0, t)$, cf. [35], which leads to an equivalent representation of G as a PDE coupled with and ODE:

$$G: \quad \begin{aligned} z_{tt}(\xi,t) &= z_{\xi\xi}(\xi,t) - 2\lambda z_t(\xi,t) \\ z(1,t) &= \widetilde{u}(t) \\ \alpha z_\xi(0,t) &= z(0,t) + (q + 2\alpha\lambda)v(t) \\ \alpha\dot{v}(t) &= z(0,t) + qv(t). \end{aligned} \tag{17}$$

Here the new state is (z, z_t, v), the measured outputs are

$$y_1 = v, \quad y_2(t) = \int_0^1 z_t(\xi, t)\, d\xi + v(t),$$

and a new control $\widetilde{u}(t) = u(t) - x_t(1, t) = u(t) - y_2(t)$ is used. Since by hypothesis the controller $u = Ky$ stabilizes (1) in the H_∞ sense, so does $\widetilde{u} = Ky - y_2$ for (17), and since the state trajectories remain unaffected, we may from here on prove the statement for controller $\widetilde{u} = Ky$ and system (17). It is also clear that we may replace the outputs y_1, y_2 by the equivalent outputs $\widetilde{y}_1 = v$, $\widetilde{y}_2 = \int_0^1 z_t(\xi, t)d\xi$, because $\widetilde{y}_1 = y_1$, $\widetilde{y}_2 = y_2 - y_1$. Then $\widetilde{u} = u - y_2 = u + \widetilde{y}_1 - \widetilde{y}_2$, and the controller is $\widetilde{u} = \widetilde{K}\widetilde{y}$. At this stage, for the ease of presentation, we drop the tilde notation and write the new control and measurements again as u and y. What has been achieved so far? Apart from the change of output variables, we have an equivalent system with state (z, z_t, v), where the trace $v = z_t(0, \cdot)$ will turn out well-defined by properly defining the domain of the differential operator in part 5).

3) Let the controller K have the form $u(s) = K(s)y(s) = K_1(s)y + K_0 y$ with direct transmission $K_0 y = k_1 y_1 + k_2 y_2$ and strictly proper $K_1(s)$. We now apply the idea of part

1) and shift its direct transmission into the plant. This leads to

$$G': \quad \begin{aligned} z_{tt} - z_{\xi\xi} + 2\lambda z_t &= 0 \\ z(1,t) &= u - k_1 y_1 - k_2 y_2 \\ \alpha z_\xi(0,t) - z(0,t) &= (q + 2\alpha\lambda) v(t) \\ \alpha \dot{v} &= qv + z(0,t) \end{aligned} \tag{18}$$

with the outputs y_1, y_2 as before, now in feedback with $u = K_1(s)y$, where K_1 is strictly proper. Note that K_1 still stabilizes (18) in the H_∞-sense, and since the state trajectories remain the same we may prove exponential stability of the loop for this pair G', K_1. Now $u(s) = K_1(s)y(s)$ gives $su(s) = sK_1(s)y(s)$, and since K_1 is strictly proper, $K'(s) := sK_1(s)$ gives a proper controller $\widehat{u}(s) := su(s) = K'(s)y(s)$, which may be represented in state space as

$$K': \quad \begin{aligned} \dot{x}_K &= A_K x_K + B_K^1 y_1 + B_K^2 y_2 \\ \widehat{u} &= C_K x_K + d_K^1 y_1 + d_K^2 y_2, \end{aligned}$$

with $\widehat{u}$ standing for the new control $\dot{u}$. Indeed, if the original state-space realization is $K = \left[\begin{array}{c|c} a & b \\ \hline c & d \end{array}\right]$, then $K_1 = \left[\begin{array}{c|c} a & b \\ \hline c & 0 \end{array}\right]$, and $K' = \left[\begin{array}{c|c} a & b \\ \hline ca & cb \end{array}\right] =: \left[\begin{array}{c|c} A_K & B_K \\ \hline C_K & D_K \end{array}\right]$. Since H_∞-stability of the loop is not altered by these transformations, we may prove the statement for the pair G', K', where the new achievement is that $K_1(s) = \frac{1}{s}K'(s)$ has integrator form, i.e., consists of a proper controller K' followed by an integrator.

4) We now perform a less standard manipulation, which consists in transferring parts of the system dynamics (18) into a new controller $\widetilde{K}$ by augmenting K' by one state. We introduce a new artificial output $y_3 = z(0,t)$ in (18), and consider the boundary wave equation

$$\widetilde{G}: \quad \begin{aligned} z_{tt} - z_{\xi\xi} + 2\lambda z_t &= 0 \\ z(1,t) &= u(t) - k_1 v - k_2 y_2 \\ \alpha z_\xi(0,t) - z(0,t) &= (q + 2\alpha\lambda) v(t) \\ y_2(t) &= \int_0^1 z_t(\xi,t)\, d\xi \\ y_3(t) &= z(0,t) \end{aligned} \tag{19}$$

Here we have substituted $v = y_1$, created a new input into $\widetilde{G}$, and have now an infinite dimensional system $\widetilde{G}$ in feedback with the augmented controller

$$\widetilde{K}: \quad \begin{aligned} \alpha \dot{v} &= qv + y_3 \\ \dot{x}_K &= A_K x_K + B_K^1 v + B_K^2 y_2 \\ \widehat{u} &= C_K x_K + d_K^1 v + d_K^2 y_2 \\ \widehat{v} &= \frac{q}{\alpha} v + \frac{1}{\alpha} y_3 \end{aligned} \tag{20}$$

where the first two equations represent the dynamics, the third and fourth equation feature the outputs $\widehat{u}, \widehat{v}$, which as we know represent $\dot{u}$ and $\dot{v}$. The ODE $\alpha\dot{v} = z(0,t) + qv = qv + y_3$ was shifted from G' into the new $\widetilde{K}$, leaving us with a simpler infinite-dimensional system $\widetilde{G}$. The controller $\widetilde{K}$ is K' augmented by this ODE, so is still finite dimensional, and moreover, is also an integral controller with regard to its new output v. The output y_1 has disappeared from (19), because the corresponding dynamics are now integrated in $\widetilde{K}$. The state of (19) is (z, z_t), while the state of $\widetilde{K}$ is (v, x_K), to which we have to add the

integrator. The significance of the fact that $\widetilde{K}$ is now an integral controller with regard to both outputs $\widehat{v} = \dot{v}$, $\widehat{u} = \dot{u}$ will become clear in the next part 5). This is required in order to comply with the way state-space representations of boundary control problems for hyperbolic equations are generated; cf. [22, p.128].

5) Our next step is to find a state-space representation of $y = \widetilde{G}[u, v]^T$ in (19), which means representing it as a well-posed boundary control system in the sense of [36, 37], [45, Def. 5.2.1] or [20]. With zero boundary conditions equation (19) reads

$$\begin{aligned} z_{tt} - z_{\xi\xi} + 2\lambda z_t &= 0 \\ z(1,t) + k_2 \int_0^1 z_t(\xi, t) d\xi &= 0 \\ \alpha z_\xi(0,t) - z(0,t) &= 0 \\ z(\xi, 0) = z_0(\xi),\ \ z_t(\xi, 0) &= z_1(t). \end{aligned}$$

This has now a representation as a strongly continuous semi-group

$$\dot{\mathfrak{z}} = \begin{bmatrix} 0 & I \\ \frac{d^2}{d\xi^2} & -2\lambda \end{bmatrix} \mathfrak{z} =: A\mathfrak{z}, \quad \mathfrak{z}(0) = \mathfrak{z}_0, \tag{21}$$

where $\mathfrak{z} = (z, z_t)$, and where the generator A has $D(A) = \{(z_1, z_2) \in H^2(0,1) \times H^1(0,1) : z_1(1) + k_2 \int_0^1 z_2(\xi, t) d\xi = 0, \alpha z_{1x}(0) - z_1(0) = 0\}$ as domain in the Hilbert space $H = H^1(0,1) \times L^2(0,1)$. Define $\mathscr{A}$ with domain $D(\mathscr{A}) = H^2 \times H^1$ by the same formula (21), and let the projector $\mathscr{P}$ with $D(\mathscr{P}) = D(\mathscr{A})$ be defined as $\mathscr{P}\mathfrak{z} = \begin{bmatrix} z_1(1) + k_2 \int_0^1 z_2(\xi) d\xi \\ \alpha z_{1\xi}(0) - z_1(0) \end{bmatrix} \in \mathbb{C}^2$, with $\mathfrak{z} = [z_1, z_2]^T$. The boundary control of $\widetilde{G}$ has now the abstract form

$$\dot{\mathfrak{z}} = \mathscr{A}\mathfrak{z}, \quad \mathscr{P}\mathfrak{z} = \begin{bmatrix} u - k_1 v \\ k_3 v \end{bmatrix}, \quad \mathfrak{y} = \mathscr{C}\mathfrak{z},$$

as in part 1), where $k_3 := q + 2\alpha\lambda$, and where $\mathfrak{y} = [y_2, y_3]$, with $\mathscr{C} : H^1 \times L^2 \to \mathbb{C}^2$ bounded. Finally we re-arrange the boundary condition by defining $\mathscr{P}'$ with $D(\mathscr{P}') = D(\mathscr{P})$ as

$$\mathscr{P}'\mathfrak{z} = \begin{bmatrix} z_1(1) + k_2 \int_0^1 z_2(\xi) d\xi + \alpha \frac{k_1}{k_3} z_{1\xi}(0) - \frac{k_1}{k_3} z_1(0) \\ \frac{1}{k_3}(\alpha z_{1\xi}(0) - z_1(0)) \end{bmatrix}, \quad \mathscr{P}'\mathfrak{z} = \begin{bmatrix} u \\ v \end{bmatrix} =: \mathfrak{u}.$$

In order to make this well defined, we have to assure, according to [22, Sect. 3.3], that $D(\mathscr{A}) \subset D(\mathscr{P}')$, $D(A) = D(\mathscr{A}) \cap \ker(\mathscr{P}')$, $A\mathfrak{z} = \mathscr{A}\mathfrak{z}$ on $D(A)$, and that A generates a C_0-semi group. These are satisfied by construction. In addition, we require an operator $B : \mathbb{C}^2 \to H$ such that $\mathscr{P}' \circ B = I$, $\mathrm{im}(B) \subset D(\mathscr{A})$ and $\mathscr{A} \circ B$ bounded. This can be arranged by the ansatz

$$B\mathfrak{u} = \begin{bmatrix} b(\cdot)u + c(\cdot)v \\ 0 \end{bmatrix}, \quad b(\xi) = b_0\xi^2 + b_1\xi + b_2, \quad c(\xi) = c_0\xi^2 + c_1\xi + c_2,$$

where equating $\mathscr{P}' \circ B \stackrel{!}{=} I$ leads to

$$\mathscr{P}'B\mathfrak{u} = \begin{bmatrix} b(1)u + c(1)v + d_K^1(\alpha b'(0)u + \alpha c'(0)v - b(0)u - c(0)v) \\ \alpha b'(0)u + \alpha c'(0)v - b(0)u - c(0)v \end{bmatrix} \stackrel{!}{=} \begin{bmatrix} u \\ v \end{bmatrix} = \mathfrak{u}$$

which allows to determine the coefficients b_i, c_i as

$$b(\xi) = \xi^2, \quad c(\xi) = (k_3 - k_1)\xi^2 - k_3.$$

As is well-known, (cf. [22, Sect. 3.3]), the boundary wave equation may now be represented by the state-space equation

$$\dot{\mathfrak{x}} = A\mathfrak{x} - B\dot{\mathfrak{u}} + \mathscr{A}B\mathfrak{u}, \quad \mathfrak{x}(0) = \mathfrak{x}_0, \tag{22}$$

where solutions $\mathfrak{z}$ of (19) and $\mathfrak{x}$ of (22) are related by $\mathfrak{x}(t) = \mathfrak{z}(t) - B\mathfrak{u}(t)$. This can be further streamlined as

$$\dot{\mathfrak{x}^e} = \begin{bmatrix} 0 & 0 \\ \mathscr{A}B & A \end{bmatrix} \mathfrak{x}^e + \begin{bmatrix} I \\ -B \end{bmatrix} \widehat{\mathfrak{u}}, \tag{23}$$

where the extended state is $\mathfrak{x}^e = (\mathfrak{u}, \mathfrak{x}) = (u, v, z, z_t)$, and where $\widehat{\mathfrak{u}} = \dot{\mathfrak{u}} = [\widehat{u}, \widehat{v}]^T$ has become the input. The output operator for (23) is now $\mathfrak{y} = \mathscr{C}^e\mathfrak{x}^e = \mathscr{C} \circ [B \;\; I] \begin{bmatrix} u \\ \mathfrak{z} - Bu \end{bmatrix} = \mathscr{C}\mathfrak{z}$. It is now clear why it was necessary to find a controller of integrator form (20), because it was necessary to comply with the form (23) of the state-space representation of a hyperbolic boundary value problem. We also note that well-posedness of the transformed system (23) implies well-posedness of the original system with state (x, x_t). See also [35, sect. 4] for this transformation.

6) We next show that system $\widetilde{G}$, and therefore also the state-space representation (23) with C_0-semi group, is exponentially stabilizable. This can for instance be obtained from [35, Theorem 4.2], where the authors construct a state feedback controller which stabilizes (17) exponentially in the Hilbert space $H = H^2 \times H^1 \times L^2$. The control law found in that reference can be arranged as a state feedback law for $\widetilde{G}$, and hence for (23), using the same technique of shifting parts of the dynamics from plant to controller. Alternatively, we may even use the open loop characterization of stabilizability, called optimizability in [49], which is equivalent to stabilizability, while offering a more convenient way to check it.

7) We now show that the controller $\widetilde{K}$ is admissible for $\widetilde{G}$ and is as a system exponentially stabilizable. Due to shifting the direct transmission of K into the plant as outlined in 1) and put to work in (19), the new controller $\widetilde{K}$ in (20) is written as an integral controller, that is, its output is $\widehat{\mathfrak{u}} = \dot{\mathfrak{u}} = [\dot{u}, \dot{v}]$, which makes it admissible for $\widetilde{G}$.

Assuming that the original $K = \left[\begin{array}{c|c} a & b \\ \hline c & d \end{array}\right]$ is stabilizable and detectable (e.g. minimal), the same is true for K' obtained in 3), so $\left[\begin{array}{c|c} A_K & B_K \\ \hline C_K & D_K \end{array}\right]$ is stabilizable. Now the augmented controller is $\widetilde{K} = \left[\begin{array}{c|c} \widetilde{A}_K & \widetilde{B}_K \\ \hline \widetilde{C}_K & \widetilde{D}_K \end{array}\right]$ with $\widetilde{A}_K = \begin{bmatrix} A_K & B_K^1 \\ 0 & \alpha^{-1} \end{bmatrix}$, $\widetilde{B}_K = \begin{bmatrix} B_K^2 & 0 \\ 0 & \alpha^{-1} \end{bmatrix}$, $\widetilde{C}_K = \begin{bmatrix} C_K & d_K^1 \\ 0 & \alpha^{-1} \end{bmatrix}$, $\widetilde{D}_k = \begin{bmatrix} d_K^2 & 0 \\ 0 & \alpha^{-1} \end{bmatrix}$. Applying the Hautus test, for simplicity in the case $\lambda \neq \alpha^{-1}$, let v be an eigenvector of A_K^T with unstable eigenvalue λ, then $[v \;\; \rho]^T$ is an eigenvector of $\widetilde{A}_K^T$ for λ if $\rho = B_K^{1T} v/(\lambda - \alpha^{-1})$. Now $\widetilde{B}_K^T[v \;\; \rho]^T = [v \;\; v(\alpha^{-1}/(\lambda - \alpha^{-1}))]^T$, and this vector cannot equal the vector $[0, \; 0]^T$, because that would imply $B_K^{1T} v = 0$ and $B_K^{2T} v = 0$, hence $B_K^T v = 0$, contradicting stabilizability of $[A_K, B_K, C_K, D_K]$. Now for the eigenvalue α^{-1} of $\widetilde{A}_K^T$ we take the eigenvector $w = [0 \; 1]^T$, then $\widetilde{B}_K^T w = [0 \; \alpha^{-1}]^T \neq [0 \; 0]^T$, which proves stabilizability.

With $\widetilde{G}$ and $\widetilde{K}$ exponentially stabilizable, the closed loop $(\widetilde{G}, \widetilde{K})$ is also exponentially stabilizable (see [45, Prop. 8.2.10(ii)(c)]) in the sense of the induced state-space realization [45, Chap. 7]. The infinitesimal generator of the closed loop will be denoted as A_{cl}.

8) Next we argue that $\widetilde{G}$ is exponentially detectable. Since $\widetilde{G}$ is exponentially stabilizable, its semi-group satisfies the spectrum decomposition assumption, see [22, Theorem 5.2.6]. Since from the discussion of section 3 we know that there are only finitely many right hand poles, all with finite multiplicity, a necessary and sufficient condition for exponential detectability is that $\ker(sI - \widetilde{A}) \cap \ker(\widetilde{C}) = \{0\}$ for every $s \in \overline{\mathbb{C}}_+$; see [22,

Theorem 5.2.11], where $(\widetilde{A}, \widetilde{B}, \widetilde{C})$ refers to the state-space realization of $\widetilde{G}$ derived in 2) above. But that may now be checked in the frequency domain. It means that for every $s \in \overline{\mathbb{C}}_+$ the only solution of the Laplace transformed system (9) with $u = 0$ satisfying $y_1(s) = sx(0,s) = 0$, $y_2(s) = sx(1,s) = 0$ is $x \equiv 0$. Now for $s \neq 0$ these boundary conditions give $x(0,s) = 0$, $x(1,s) = 0$, and therefore from the boundary conditions in (9) $x_\xi(0,s) = 0$, $x_\xi(1,s) = 0$. The general solution of the dynamic equation in (9) being $x(\xi,s) = k_1 e^{\sigma\xi} + k_2 e^{-\sigma\xi}$, with constants depending on s, we get the four conditions $k_1 + k_2 = 0$, $\sigma(k_1 - k_2) = 0$, $k_1 e^{\sigma} + k_2 e^{-\sigma} = 0$, $\sigma(k_1 e^{\sigma} - k_2 e^{-\sigma}) = 0$, which can only be satisfied if $k_1 = k_2 = 0$.

With $\widetilde{G}$ exponentially detectable, and $\widetilde{K}$ exponentially detectable with an argument similar to 7) above, the closed loop is exponentially detectable, again by [45, Prop. 8.2.10(ii)(c)].

9) We have now arrived at the crossroad, where the successive transformations $(G, K) \to (G', K') \to (\widetilde{G}, \widetilde{K})$ bear fruit. Namely, according to [26, Theorem 5.2], a well-posed system which is exponentially stabilizable, exponentially detectable, and at the same time H_∞-stable, is already exponentially stable in the state-space sense, i.e., the generator of its semi-group is exponentially stable. We apply this to the closed loop system $(\widetilde{G}, \widetilde{K})$ with generator A_{cl}. For this result see also [49, Thm. 1.1], and [29, 8.35] for a classical antecedent. □

Corollary 2. *Let K be a finite-dimensional controller for* (1)-(2)*, and suppose the closed loop with the linearization G of* (1) *has no unstable poles. Then K stabilizes G exponentially and $G_{\rm nl}$ locally exponentially.*

Proof: The result follows from Theorem 2 above, once we show that $\widetilde{K}$ in (20) stabilizes $\widetilde{G}$ in (19) in the H_∞-sense. Since the transfer functions are not concerned by the transformations in the proof of Theorem 2, it suffices to show that K stabilizes G in the H_∞-sense. For that we have to show that the closed loop transfer operator

$$T(s) = \begin{bmatrix} I & G(s) \\ -K(s) & I \end{bmatrix}^{-1} = \begin{bmatrix} (I+KG)^{-1} & -K(I+GK)^{-1} \\ (I+GK)^{-1}G & (I+GK)^{-1} \end{bmatrix} \in \mathbf{H}_\infty$$

belongs to the Hardy space $\mathbf{H}_\infty$. Since we know by hypothesis that $T(s)$ has no poles in $\overline{\mathbb{C}}_+$, this follows as soon as T is bounded on $j\mathbb{R}$. Since K is proper, this hinges on the behavior of G on $j\mathbb{R}$. As is easy to see, the denominator $d(s)$ of (10) satisfies $\lim_{\omega\to\infty} |d(j\omega)| = \infty$, so $y_1(s)/u(s)$ is proper, and it remains to show that $y_2(s)/u(s)$ in (10) is bounded on $j\mathbb{R}$. Dividing numerator and denominator of n_2/d in (9) by $(e^{\sigma} - e^{-\sigma})/2\sigma$, and observing that the term $\frac{(e^{\sigma}+e^{-\sigma})/2}{(e^{\sigma}-e^{-\sigma})/2\sigma}$ is bounded on $j\mathbb{R}$, we see that $y_2(s)/u(s)$ is bounded, because the leading terms in both numerator and denominator are now $\alpha s^2 = -\alpha\omega^2$. That proves H_∞-stability of the closed loop hence exponential stability of the linear closed loop.

It remains to show that K stabilizes $G_{\rm nl}$ locally exponentially. Due to the specific form of the non-linearity, this may be obtained with [53]. □

Remark 2. Semi-groups for hyperbolic equations with boundary dynamics have been investigated, e.g. in [31], but as this requires additional conditions, we believe that our method of simplifying the infinite-dimensional part by augmenting the controller offers additional flexibility. After all the goal is to show that the closed-loop has an exponentially stabilizable and detectable semi-group $e^{A_{cl}t}$, not necessarily the individual parts.

Remark 3. For finite-dimensional systems arbitrary decay rates in closed loop can be achieved by observer-based controllers under controllability and observability assumptions. For infinite-dimensional systems it is already more challenging to achieve arbitrary exponential decay even by state feedback, see e.g. [43].

The situation changes thoroughly with structured controllers, where even in finite dimensions arbitrary decay rates may no longer be possible. One should, however, bear in mind that optimizing the decay rate is by itself not a reasonable tuning goal. This leads to high gain controllers, which are very sensitive to model errors. This is one of the reasons why robust control is nowadays preferred in practice. A further reason is that requiring arbitrarily fast decay rates needs assignment of the real parts of all closed-loop eigenvalues, which is no longer possible e.g. when actuator or sensor dynamics are present in the model, again underlining the academic nature of this problem.

The merit of Theorem 2 is that from now on exponential stability of the loop (G, K) between the infinite-dimensional system G in (1)-(2) with any finite-dimensional controller K can be checked via the Nyquist test. What remains to be done is actually *find* such a stabilizing controller. A straightforward idea is to use a discretization of (1), the most obvious being finite differences

$$x_i(t) = x(\xi_i, t), \xi_i = ih, i = 0, \dots, N, Nh = 1$$
$$x_\xi(\xi_i, t) \approx \frac{x_{i+1}(t) - x_{i-1}(t)}{2h},\ x_{\xi\xi}(\xi_i, t) \approx \frac{x_{i+1}(t) + x_{i-1}(t) - 2x_i(t)}{h^2}.$$

With the boundary condition at $\xi = 0$

$$\alpha x_0''(t) = \frac{x_1(t) - x_{-1}(t)}{2h} + q x_0'(t)$$

we can eliminate x_{-1}, and with the boundary condition at $\xi = 1$

$$\frac{x_{N+1}(t) - x_{N-1}(t)}{2h} = -x_N'(t) + u(t)$$

we eliminate x_{N+1}. Putting $\tilde{x}_i = x_i'$, $i = 0, \dots, N$, we get a dynamical system of order $2N + 2$

$$\begin{bmatrix} x' \\ \tilde{x}' \end{bmatrix} = \begin{bmatrix} 0 & I \\ T & \Lambda \end{bmatrix} \begin{bmatrix} x \\ \tilde{x} \end{bmatrix} + \begin{bmatrix} 0 \\ b \end{bmatrix} u, \quad y_1(t) = \tilde{x}_0(t), y_2(t) = \tilde{x}_N(t), \tag{24}$$

with typical A-matrix featuring a tridiagonal T and a diagonal Λ. It comes as a mild surprise that (24) is not stabilizable, the reason being a pole/zero cancellation at the origin.

Kalman reduction using the function `minreal` from [54] removes one state of (24) and furnishes a stabilizable system, which we use for synthesis, and where the reduced system A-matrix is now no longer sparse. In our experiment we chose $N = 50$ and synthesized controllers of various simple structures like a sum of PIDs $u = \mathtt{PID}_1 y_1 + \mathtt{PID}_2 y_2$, a 5th-order state-space controllers, or on ignoring one of the outputs, standard PID controllers $u = \mathtt{PID}\, y_1$, respectively, $u = \mathtt{PID}\, y_2$. These controllers, once they stabilize the reduced finite-dimensional system, are then tested against the infinite dimensional system using the Nyquist test of [5], which by Corollary 2 gives an exact answer. For instance, stabilizing the gray and blue scenarios with the 5th-order controller given in (31) leads to the Nyquist plots in Fig. 4 for the gray and blue scenarios, and certifies infinite-dimensional stability.

As can be seen, in the blue case (right) the Nyquist curve winds twice around the origin. Since K_{blue} is stable and the open loop G_{blue} has $n_p = 2$ unstable poles, this proves

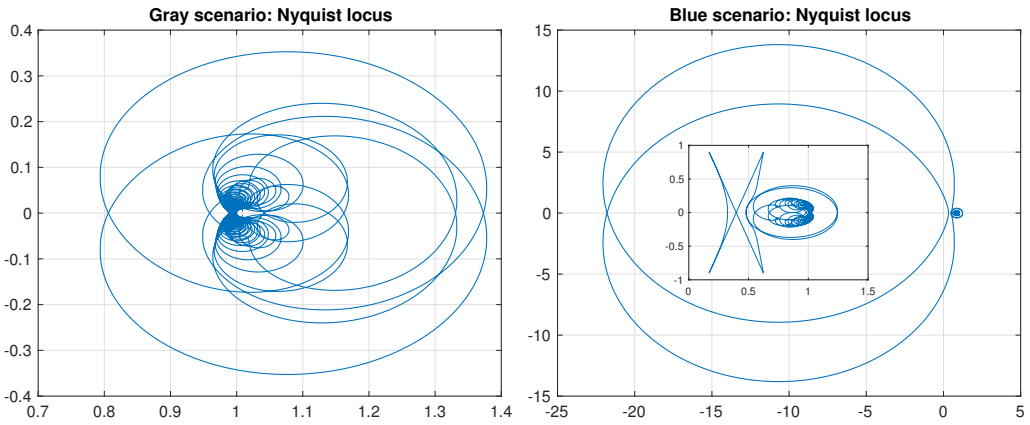

FIGURE 4. Nyquist curve $1 + K_{\text{blue}}G_{\text{blue}}$ (right) winds twice around origin. Since K_{blue} is stable and $n_p = 2$, closed loop is certified exponentially stable. Gray case (left) has $n_p = 0$ and winding number 0 around origin (critical point). Since K_{gray} is stable, loop is certified exponentially stable.

exponential stability of the closed-loop $(G_{\text{blue}}, K_{\text{blue}})$. At this point we have completed step 2 of the general synthesis algorithm 1.

Remark 4. The fact that finite-difference and finite-element discretizations of stabilizable (or detectable) hyperbolic equations may turn out not stabilizable (detectable) cannot be overcome by increasing N. This has been the cause of a large body of controllability literature, which fortunately has little relevance for control. Namely, once we have decided that the true model for the drilling process is the infinite-dimensional (1)-(2), we little care whether K, synthesized for G and G_{nl}, also stabilizes discretizations of G or G_{nl}.

6. H_∞-SYNTHESIS

The final step in algorithm 1 is H_∞-synthesis. While we have already shown that the non-linear system can be locally exponentially stabilized by a finite-dimensional controller, we now strive to prove global exponential stability of the closed-loop system (G_{nl}, K). In the following, it is helpful to represent the non-linear system G_{nl} in Lur'e form, i.e., as the closed loop interconnection of its linearization with a static non-linearity.

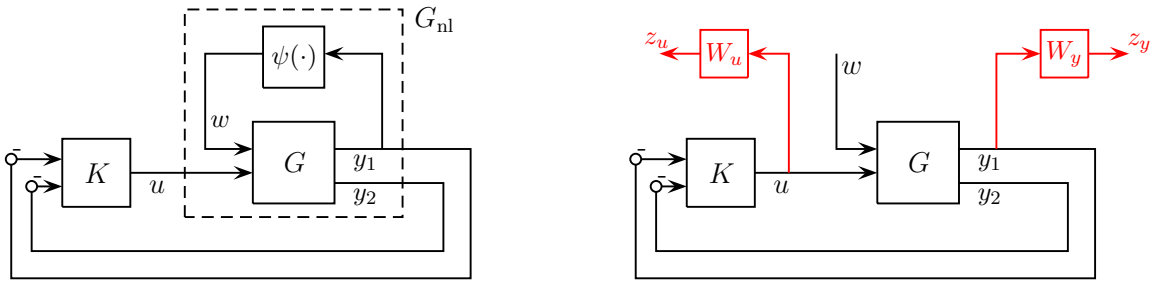

FIGURE 5. Non-linear system (left) in feedback form. The synthesis interconnection (right) interprets non-linearity as an exogenous disturbance w.

6.1. **Mixed sensitivity.** The non-linear system can be consider as a feedback loop between the linearized plant

$$
\begin{aligned}
x_{tt}(\xi,t) &= x_{\xi\xi}(\xi,t) - 2\lambda x_t(\xi,t)\\
x_\xi(1,t) &= -x_t(1,t) + u(t)\\
\alpha x_{tt}(0,t) &= x_\xi(0,t) + q x_t(0,t) + w(t)\\
y_1(t) = x_t(0,t), y_2(t) &= x_t(1,t), z = (y,u),
\end{aligned}
\qquad P: \tag{25}
$$

connected with the controller $u = Ky$ and the non-linearity $\psi(\cdot)$ as in Fig. 5 left. We now have several choices. The most straightforward one is to grossly interpret the non-linearity $\psi(x_t(0,t))$ as a disturbance w, forgetting its specific form. In (25) we then introduce typical outputs like $z_y = W_y y$, $z_u = W_u u$, where the channel $w \to z_y$ rejects the effect of the non-linearity on the low-frequency part of the measured output, while $w \to W_u u = z_u$ accounts for high frequency components of the control signal, so that minimizing the H_∞-norm of $T_{wz}(K)$ limits the degrading effects of the non-linearity while maintaining reasonable control authority. Here and for the following $T_{ab}(K)$ denotes a closed-loop channel $b \to a$ in plant P. The closed loop of (25) with K from w to z is obtained as $T_{zw}(K) = \mathrm{diag}(W_u, W_y) T_{(u,y),w}(K)$ as shown in Fig. 5 right.

6.2. **Sector non-linearity.** A more sophisticated approach uses the fact that the non-linearity ψ in (7) induced by $\phi = \phi_{\text{mud}} + \phi_{\text{rock}}$ as in (8) is sectorial. That is to say, there exist $q_l \le q_u$ such that $q_l\omega \le \psi(\omega) \le q_u\omega$ for all ω, i.e., (1) is an infinite dimensional Lur'e system. For the scenarios gray and blue these sectors are shown in Fig. 6.

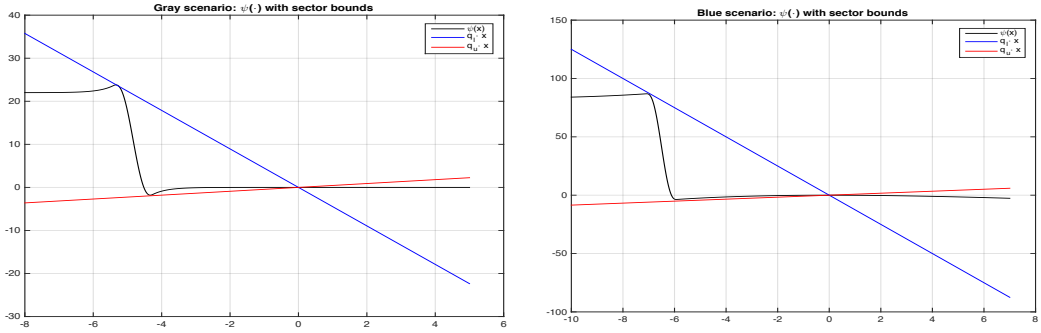

FIGURE 6. Sector non-linearity $q_l\omega \le \psi(\omega) \le q_u\omega$ for gray scenario (left) and blue scenario (right).

Lemma 4. *For $\omega \to \pm\infty$ the non-linearity $\psi(\omega)$ behaves asymptotically like a line $-q_s\omega + a_\pm$, where*

$$
q_s = \frac{c_b}{\sqrt{GJI}} + q,\quad a_+ = \frac{LW_{ob}R_b}{GJ}(\mu_{sb} - \mu_{cb})e^{-\frac{\gamma_b}{\nu_f}\Omega},\quad a_- = 2\frac{LW_{ob}R_b\mu_{cb}}{GJ} + \frac{L}{GJ}\left(\mu_{cb} - \mu_{sb}\right)e^{-\frac{\gamma_b}{\nu_f}\Omega}.
$$

Proof: Note that since we have transferred the steady state to the origin, the kink of the friction term $\psi(\omega)$ occurs at $\omega = -\frac{L\Omega\sqrt{I}}{\sqrt{GJ}} =: -\omega_0$. For $\omega \gg -\omega_0$ we have $\psi(\omega) = -(\frac{c_b}{\sqrt{GJI}} + q)\omega + \frac{LW_{ob}R_b}{GJ}(\mu_{sb} - \mu_{cb})e^{-\frac{\gamma_b}{\nu_f}\Omega}(1 - e^{-\frac{\gamma_b}{\nu_f}\frac{1}{L}\sqrt{\frac{GJ}{I}}\omega}) \sim -(\frac{c_b}{\sqrt{GJI}} + q)\omega + \frac{LW_{ob}R_b}{GJ}(\mu_{sb} - \mu_{cb})e^{-\frac{\gamma_b}{\nu_f}\Omega} = -q_s\omega + a_+$, and for $\omega < -\omega_0$ we get $\psi(\omega) = -(\frac{c_b}{\sqrt{GJI}} + q)\omega + 2\frac{LW_{ob}R_b\mu_{cb}}{GJ} + \frac{L}{GJ}\left(\mu_{cb} - \mu_{sb}\right)e^{-\frac{\gamma_b}{\nu_f}\Omega} + \frac{L}{GJ}\left(\mu_{cb} - \mu_{sb}\right)e^{-\frac{1}{L}\sqrt{\frac{GJ}{I}}|\omega|}e^{\frac{\gamma_b}{\nu_f}\Omega}\Big) \sim -(\frac{c_b}{\sqrt{GJI}} + q)\omega + 2\frac{LW_{ob}R_b\mu_{cb}}{GJ} + \frac{L}{GJ}\left(\mu_{cb} - \mu_{sb}\right)e^{-\frac{\gamma_b}{\nu_f}\Omega} = -q_s\omega + a_-$. □

Since both branches behave asymptotically like a line with slope

$$-q_s := -\frac{c_b}{\sqrt{GJI}} - q = -\frac{W_{ob}R_b(\gamma_b/\nu_f)(\mu_{sb}-\mu_{cb})e^{-\frac{\gamma_b}{\nu_f}\Omega}}{\sqrt{GJI}}, \tag{26}$$

it is not hard to find slopes q_l, q_u with $q_l\omega \le \psi(\omega) \le q_u\omega$. Those can be seen in Fig. 6 for the gray and blue cases. We use the standard notation $\psi \in \mathbf{sect}(q_l, q_u)$.

In order to achieve stability of the non-linear closed loop, we now apply the technique of Zames [50], which requires that the linear system $T_{y_1w}(K)$ in feedback with the non-linearity $\psi(\cdot)$ as in Fig. 5 left satisfy the complementary sector constraint. To put this to work, we let $c = (q_l + q_u)/2$ and $r = (q_u - q_l)/2$, and introduce the centered non-linearity $\chi(w) = \psi(w) - cw$, which satisfies $\chi \in \mathbf{sect}(-r, r)$.

The centered non-linearity $\chi(w) = \psi(w) - cw$ is now in feedback with the following shifted plant:

$$\widetilde{P}: \quad \begin{aligned} x_{tt}(\xi,t) &= x_{\xi\xi}(\xi,t) - 2\lambda x_t(\xi,t) \\ x_\xi(1,t) &= -x_t(1,t) + u(t) \\ \alpha x_{tt}(0,t) &= x_\xi(0,t) + (q+c)x_t(0,t) + e(t) \\ y_1(t) &= x_t(0,t), y_2(t) = x_t(1,t), z(t) = x_t(0,t), \end{aligned} \tag{27}$$

connected with

$$u = Ky, \quad z_\chi = \chi(e_\chi), \quad e = z_\chi + w, \quad e_\chi = z + w_\chi. \tag{28}$$

Closing the loop with regard to $u = Ky$ leads to $z = \widetilde{T}_{ze}(K)e$, which is in loop with the non-linearity $z_\chi = \chi(e_\chi)$ as in Fig. 7. Here and in the following channels derived form plant $\widetilde{P}$ will be denoted $\widetilde{T}_{wz}(K)$ etc. Note that the sole difference between P and $\widetilde{P}$ is that the parameter q is replaced by $\widetilde{q} = q + c$. In particular, stabilization of $\widetilde{P}$ is obtained as studied in section 5. Ultimately this means that K will have to stabilize the linear wave equation for two different values $q, \widetilde{q}$, while α, λ remain fixed.

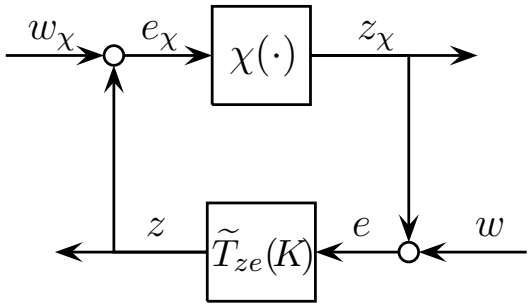

FIGURE 7. Closing the loop with $u = Ky$ in (27) leaves an exponentially stable linear system $\widetilde{T}_{ze}(K)$ in feedback with the shifted static non-linearity $z_\chi = \chi(e_\chi)$.

Lemma 5. *Let $\psi \in \mathbf{sect}(q_l, q_u)$ and put $c = (q_u + q_l)/2$, $r = (q_u - q_l)/2$. Suppose the controller K has been tuned such that the closed loop $(\widetilde{P}, K)$ is H_∞-stable with $\|\widetilde{T}_{ze}(K)\|_\infty < r^{-1}$. Then the non-linear closed-loop (1) with $u = Ky$ is finite gain input-output stable, i.e., there exists a constant $M > 0$ such that in (27)-(28) we have $\|x_t(0,\cdot)\|_2 + \|\psi(x_t(0,\cdot))\|_2 \le M\,(\|w_\chi\|_2 + \|w\|_2)$ for all inputs $w, w_\chi \in L^2[0,\infty)$.*

Proof: This follows from [50, Thm. 1]. If $\psi \in \mathbf{sect}(q_l, q_u)$, then the centered non-linearity $\chi := \psi - cI$ satisfies $\chi \in \mathbf{sect}(-r, r)$, hence $\|\chi(z_\chi)\|_2 \leq r\|z_\chi\|_2$ has L^2-gain r in the sense of [50, Def. (3)]. This non-linearity is now in feedback with $\widetilde{T}_{ze}(K)$. Since by assumption K has been tuned such that $\|\widetilde{T}_{ze}(K)\|_\infty < r^{-1}$, this LTI-system has L^2-gain $< r^{-1}$, and the small gain theorem implies boundedness of the loop (27)-(28), i.e., there exists a constant $M > 0$ such that $\|e_\chi\|_2 \leq M(\|w\|_2 + \|w_\chi\|_2)$ and $\|e\|_2 \leq M(\|w\|_2 + \|w_\chi\|_2)$ in Fig. 7. Since in closed loop the input e to $\widetilde{T}_{ze}(K)$ represents the non-linear term $\chi(x_t)$, we derive $\|\chi(x_t(0,\cdot))\|_2 \leq M\left(\|w_\chi\|_2 + \|w\|_2\right)$. Still from the small gain theorem we get $\|e_\chi\|_2 \leq M\left(\|w_\chi\|_2 + \|w\|_2\right)$, and since in closed loop e_χ represents the output $x_t(0,\cdot)$, we have $\|x_t(0,\cdot)\|_2 \leq M\left(\|w_\chi\|_2 + \|w\|_2\right)$ in closed loop. Finally, for $\psi = \chi + cI$ we get a similar estimate by combining the previous two: $\|\psi(x_t(0,\cdot))\|_2 \leq \|\chi(x_t(0,\cdot))\|_2 + c\|x_t(0,\cdot)\|_2 \leq M(1+c)\left(\|w_\chi\|_2 + \|w\|_2\right)$. □

This has now the following consequence:

Proposition 2. *Let $\psi \in \mathbf{sect}(q_l, q_u)$ with c, r as above, and suppose the controller K has been tuned such that the closed loop $(\widetilde{P}, K)$ is H_∞-stable with $\|\widetilde{T}_{ze}(K)\|_\infty < r^{-1}$. Then the non-linear closed loop between (1) and $u = Ky$ is input-to-state stable in the following sense: If the input signal $w \in L^2[0,\infty)$, then the state (x, x_t) of the non-linear closed loop with initial condition $x_{cl}(0) = x_0$ is in $L^2([0,\infty), H)$.*

Proof: Write the non-linear closed loop in the abstract state-space H in theorem 2 as $\dot{x}_{cl} = A_{cl}x_{cl} + \Psi(x_{cl}) + w$, $x_{cl}(0) = x_0$, where A_{cl} is exponentially stable, $\Psi(x_{cl}) = \psi(x_t(0,\cdot))$ for the closed-loop $x_t(0,t)$, and where $w(t)$ is an input to the equation $\alpha x_{tt}(0,t) = x_\xi(0,t) + qx_t(0,t) + \psi(x_t(0,t))$. The linear feedback system $(\widetilde{P}, K)$, respectively its channel $\widetilde{T}_{ze}(K)$, is now $\dot{x}_{cl} = A_{cl}x_{cl} + e$, $z = C_{cl}x_{cl}$, in loop with the centered non-linearity $\chi(\cdot)$, and w is the lower right input in Fig. 7. To account for a non-zero initial condition $x_{cl}(0) = x_0$ we choose the top left input in Fig. 7 as $w_\chi = C_{cl}e^{A_{cl}t}x_0$, where C_{cl} is the output operator of closed loop system $(\widetilde{P}, K)$. Then e_χ is the solution of the Cauchy problem $\dot{x}_{cl} = A_{cl}x_{cl} + e, x_{cl}(0) = x_0$. From the lemma we get $\|\Psi(x_{cl})\|_2 = \|\psi(x_t)\|_2 \leq M\left(\|w_\chi\|_2 + \|w\|_2\right) \leq M'\left(\|x_{cl}(0)e^{-\omega_0 t}\|_2 + \|w\|_2\right)$, where $-\omega_0 < 0$ is the growth rate of the exponentially stable generator A_{cl}. In particular, if we put $v(t) = \Psi(x_{cl}(t)) + w(t)$, then $\|v\|_2 \leq (M'+1)\left(|x_{cl}(0)| + \|w\|_2\right)$, hence we may consider $v(t)$ as a right hand side in L^2 to the non-homogeneous Cauchy problem $\dot{x}_{cl} = A_{cl}x_{cl} + v$, $x_{cl}(0) = x_0$. Since A_{cl} is exponentially stable, the closed loop state is then also in L^2; [29, Ch. VI,7.1a]. □

One wonders whether the state $x_{cl}(t)$ decays exponentially to 0 when this is the case for the input $w(t)$. Suppose $w \in L^2$ decays exponentially in the sense that $w = e^{-at}\widetilde{w}$ for some $a > 0$ and $\widetilde{w} \in L^2$. In this case it seems plausible to work with the weighted squared L^2-norm $|||w|||_2^2 = \|e^{at}w(\cdot)\|_2^2 = \|\widetilde{w}\|_2^2$.

Proposition 3. *Suppose $\psi \in \mathbf{sect}(q_l, q_u)$ with c, r as above, and suppose K has been tuned such that $(\widetilde{P}, K)$ is H_∞-stable, with $\|\widetilde{T}_{ze}(K)\|_\infty < r^{-1}$. There exists $a > 0$ such that whenever the input w decays exponentially with rate at least as fast as a, i.e., $w(t) = e^{-at}\widetilde{w}(t)$ for some $\widetilde{w} \in L^2[0,\infty)$, then the state $x_{cl}(t)$ of the non-linear closed loop in response to the input w decays exponentially with rate at least a.*

Proof: 1) Since the closed loop $(\widetilde{P}, K)$ is exponentially stable with $-\omega_0 := \omega_0(A_{cl}) < 0$ and $\|\widetilde{T}_{ze}(K)\|_\infty < r^{-1}$, we may choose a small enough shift $0 < a < \omega_0$ such that

$(\widetilde{P}(\cdot - a), K(\cdot - a))$ is still exponentially stable and $\|\widetilde{T}_{ze}(K)(\cdot - a)\|_\infty < r^{-1}$. Let $|||\cdot|||_2$ be the corresponding weighted L^2-norm as above.

2) Let us observe that for the centered non-linearity $\chi \in \mathbf{sect}(-r, r)$ implies $|||\chi(w)|||_2 \leq r\,|||w|||_2$ for all $w = e^{at}\widetilde{w}$. Namely, $|||\chi(w)|||_2^2 = \int_0^t e^{2a\tau}|\chi(w(\tau))|^2 d\tau \leq \int_0^t e^{2a\tau} r^2 |w(\tau)|^2 d\tau = r^2\,|||w|||_2^2$.

3) Now we establish the complementary estimate for the LTI feedback system $(\widetilde{P}, K)$ and its channel $\widetilde{T}_{ze}(K)$ with regard to the norm $|||\cdot|||_2$. We have

$$\begin{aligned}
|||\widetilde{T}_{ze}(K) * w|||_2^2 &= \int_0^\infty e^{2at}\left|\int_0^t \widetilde{T}_{ze}(K)(t-\tau)w(\tau)d\tau\right|^2 dt \\
&= \int_0^\infty \left|\int_0^t \widetilde{T}_{ze}(K)(t-\tau)e^{a(t-\tau)}w(\tau)e^{a\tau}d\tau\right|^2 dt \\
&= \int_0^\infty \int_0^t \left|\left(\widetilde{T}_{ze}(K)\cdot e^{at}\right)(t-\tau)\left(w\cdot e^{at}\right)(\tau)d\tau\right|^2 dt \\
&= \|(\widetilde{T}_{ze}(K)\cdot e^{at}) * \widetilde{w}\|_2^2 = \|\widetilde{T}_{ze}(K)(s-a)\cdot\widetilde{w}(s)\|_2^2 \\
&\leq \|\widetilde{T}_{ze}(K)(\cdot - a)\|_\infty^2 \|\widetilde{w}\|_2^2 = \|\widetilde{T}_{ze}(K)(\cdot - a)\|_\infty^2\,|||w|||_2^2 \\
&< r^{-2}\,|||w|||_2^2\,.
\end{aligned}$$

This means we may apply the small gain argument with the norm $|||\cdot|||_2$. The result is as before that $|||x_t(0,\cdot)|||_2 + |||\psi(x_t(0,\cdot))|||_2 \leq M\,(|||w_\chi|||_2 + |||w|||_2)$ for some $M > 0$ and all inputs $w = e^{-at}\widetilde{w}$, $w_\chi = e^{-at}\widetilde{w}_\chi$ with $\widetilde{w}, \widetilde{w}_\chi \in L^2[0,\infty)$. That means the non-linearity in closed loop in response to the signal $w = e^{-at}\widetilde{w}$ also decays at least as fast as e^{-at}, so that the right hand side $v(t) = \Psi(x_{cl}(t)) + w(t)$ already used in the previous proposition is of the form $v(t) = e^{-at}\widetilde{v}(t)$ for some $\widetilde{v} \in L^2$.

We also have to argue that $w_\chi = C_{cl}e^{A_{cl}t}x_0$ decays with rate a, which holds since $a < -\omega_0(A)$. But now all we have to observe is that due to exponential stability of A_{cl} in the non-homogeneous Cauchy problem $\dot{x}_{cl} = A_{cl}x_{cl} + v$ the state decays exponentially as soon as v decays exponentially. The mild solution in the semi-group sense [29, p. 436] satisfies $x_{cl}(t) = e^{A_{cl}t}x_{cl}(0) + \int_0^t e^{A_{cl}(t-\tau)}v(\tau)d\tau$, hence $|x_{cl}(t)| \leq M\left(e^{-\omega_0 t} + \|\widetilde{v}\|_2 \int_0^t e^{-\omega_0(t-\tau)}e^{-a\tau}d\tau\right) \leq M(1 + \|\widetilde{v}\|_2/(\omega_0 - a))e^{-at}$. □

This brings us now to our first optimization program, where we combine a mixed H_∞ performance and robustness requirement (Fig. 5 right) for the nominal plant with a sector constraint assuring global exponential stability of the non-linear closed loop (Fig. 5 left) when satisfied:

$$\begin{array}{ll} \text{minimize} & r\|\widetilde{T}_{ze}(K)\|_\infty \\ \text{subject to} & \|W_u T_{uw}(K)\|_\infty \leq 1 \\ & K \in \mathscr{K} \end{array} \tag{29}$$

Here $\mathscr{K}$ refers to a class of structured controllers, and optimization over $K \in \mathscr{K}$ can be dispensed with as soon as the objective attains a value < 1. As our experiments show, the sectorial approach works successfully for the gray scenario. Note that it is implicit in (29) that K has to stabilize P and $\widetilde{P}$, which means stabilizing the wave equation for the two different values q and $\widetilde{q} = q + c$ with the same α, λ.

6.3. **Large magnitude sector constraint.** The limitation of the sector approach is obviously that if the primal sector $\mathbf{sect}(q_l, q_u)$ is large, it is difficult to tune K such that the closed loop system (P, K) is in the complementary sector. In the transformed

metric, if the primal sector is large, then r is large, so r^{-1} is small and the constraint $\|\widetilde{T}_{ze}(K)\|_\infty < r^{-1}$ in (29) is difficult to achieve – if at all. This fails indeed for the blue scenario, and Zames-Falb multipliers [51] do not help for the specific non-linearity ψ. However, the particular structure of the non-linearity in Lemma 4 suggests the following definition as a remedy.

We say that ψ satisfies a *large magnitude sector* constraint, denoted $\psi \sim \mathbf{sect}(q_l, q_u)$, if there exist constants $L, M > 0$ such that $(\psi(x) - q_l x) \cdot (\psi(x) - q_u x) \geq 0$ for all $|x| > M$, while $|\psi(x)| \leq L|x|$ for $|x| \leq M$. A *strict* large magnitude sector is defined analogously. This is indeed what happens for $\psi(\cdot)$ here, because from Lemma 4 it follows that any choice $q_l < -q_s < q_u$ will give such a large magnitude sector.

The following result uses the peak-gain norm, which is the time-domain L_∞ operator norm $\|G\|_{\mathrm{pk\_gn}} = \sup_{|w|_\infty \leq 1} |G * w|_\infty$ of a transfer function G, with $*$ denoting convolution in the time domain, and $|\cdot|_\infty$ standing for the time-domain supremum norm on $L_\infty[0,\infty)$. See [16, 5.2.5] or [10].

Proposition 4. *Suppose ψ satisfies a large magnitude sector constraint $\psi \sim \mathbf{sect}(q_l, q_u)$ with constants L, M. Let $c = (q_u + q_l)/2$, $r = (q_u - q_r)/2$, and suppose the controller K has been tuned such that the loop $(\widetilde{P}, K)$ is H_∞-stable and satisfies $\|\widetilde{T}_{ze}(K)\|_{\mathrm{pk\_gn}} < r^{-1}$ for the peak-gain norm. Then for every input $w \in L_\infty[0,\infty)$ the non-linear closed loop state trajectory $x_{cl}(t)$ is in $L_\infty([0,\infty), H)$.*

Proof: 1) As before let $\chi = \psi - cI$ be centered, then $|\chi(x)| \leq r|x|$ for all $|x| > M$, while $|\chi(x)| \leq (L+c)|x|$ for $|x| \leq M$. We show that this implies $|\chi(w)|_\infty \leq r|w|_\infty + k$ for some constant $k > 0$ and all $w \in L_\infty[0,\infty)$ in the time domain. Indeed,

$$\begin{aligned}\sup_{t>0} |\chi(w(t))| &\leq \sup_{|w(t)|>M} |\chi(w(t))| + \sup_{|w(t)|\leq M} |\chi(w(t))| \\ &\leq \sup_{|w(t)|>M} r|w(t)| + \sup_{|w(t)|\leq M} (L+c)|w(t)| \\ &\leq r|w|_\infty + (L+c)M =: r|w|_\infty + k.\end{aligned}$$

Note that the same also holds in the truncated version, i.e., $|\chi(w)\cdot \mathbf{1}_{[0,t]}|_\infty \leq r|w\cdot \mathbf{1}_{[0,t]}|_\infty + k$ for every $t > 0$ and all w.

2) Note that by the above definition of the peak-gain norm of a transfer function $\|\widetilde{T}_{ze}(K)\|_{\mathrm{pk\_gn}} < r^{-1}$ means $|\widetilde{T}_{ze}(K) * w|_\infty \leq (r^{-1} - \delta)|w|_\infty$ for some small $\delta > 0$ for all $w \in L_\infty[0,\infty)$, and similarly in the truncated version.

3) But now both $\widetilde{T}_{ze}(K)$ and the non-linearity $\chi(\cdot)$ are finite-gain stable in the sense e.g. of [30, Def. 3] with regard to $|\cdot|_\infty$. Namely $|\chi(w)|_\infty \leq r|w|_\infty + k$ and $|\widetilde{T}_{ze}(K) * w|_\infty \leq (r^{-1} - \delta)|w|_\infty$, both fully and in the truncated version. Since $r \cdot (r^{-1} - \delta) < 1$, it follows from [30, Cor. 1] that the closed loop of Fig. 7 is finite-gain stable in the sense that $|z|_\infty \leq M(|w|_\infty + |w_\psi|_\infty) + k$ and $|z_\psi|_\infty \leq M(|w|_\infty + |w_\psi|_\infty) + k$ for certain $M, k > 0$. We derive as before that $|x_t(0,\cdot)|_\infty \leq M(|w|_\infty + |w_\chi|_\infty) + k$ and $|\psi(x_t(0,\cdot))|_\infty \leq M(|w|_\infty + |w_\chi|_\infty) + k$ for all $w \in L_\infty$, where $x_t(0,\cdot)$ is with regard to the closed loop.

4) Putting $\Psi(x_{cl}(t)) = \psi(x_t(0,t))$ and $v(t) = \Psi(x_{cl}(t)) + w(t)$ as before, we can consider $v(t)$ as a right hand side in the non-homogeneous Cauchy problem $\dot{x}_{cl} = A_{cl}x_{cl} + v$. Accounting for non-zero initial data needs $w_\chi(t) = C_{cl}e^{A_{cl}t}x_0$. Since $w \in L_\infty$, we have $|v\cdot \mathbf{1}_{[0,t]}|_\infty \leq (M+1)(|w|_\infty + |w_\chi|_\infty) + k =: k'$ for all t, and since v is square integrable up to time t, i.e., $v \cdot \mathbf{1}_{[0,t]} \in L^2[0,t]$, the solution x_{cl} exists on $[0,t]$ and is bounded independently of t by a constant depending only on k' and the decay rate $\omega_0(A_{cl})$ of A_{cl}. This gives $x_{cl} \in L_\infty$ as desired, and the solution exists at all times $t > 0$. □

Remark 5. It is clear that the impact of this result hinges on computing K for a sufficiently large sector where the constant k is as small as possible, as that controls how far the trajectory $x_{cl}(t)$ may remove herself from the steady state 0.

6.4. **Overshoot.** It has been suggested in the literature that slip-stick is avoided as soon as the non-linear system is globally stabilized. This is obviously misleading, as any sufficiently strong disturbance will cause the trajectory x_t to attain the value $-x_t^0$, however stable the loop. Stability would then only make the difference that the trajectory, after being stuck, returns to steady state when the effect of the disturbance ceases, while an unstable design might remain stuck. Since the non-linearity $\psi(\cdot)$ is concave in the neighborhood of 0, the term $qx_t + \psi(x_t) = (q + \frac{1}{2}px_t)x_t + \mathrm{o}(x_t^2) < qx_t$ is slightly below the linearized term qx_t, so that a linear controller may overestimate its effect. This may cause overshoot in the response to a disturbance, thereby increasing the risk of slip-stick. That in turn suggests optimizing the closed loop against overshoot in the channel $w \to y_1$, which we realize by simply minimizing the (unweighted) H_∞-norm of $T_{y_1w}(K)$. Reduction of peak-gain over frequency is known to be a suitable approach for systems with dominant second-order characteristics and performs equally well in the present case. In combination with the large magnitude sector this leads now to the program

$$\begin{array}{ll} \text{minimize} & \|T_{y_1w}(K)\|_\infty \\ \text{subject to} & \|\widetilde{T}_{ze}(K)\|_{\mathrm{pk\_gn}} \le 1/r \\ & \|W_uT_{uw}(K)\|_\infty \le 1 \\ & K \in \mathscr{K} \end{array} \tag{30}$$

where $T_{y_1w}(K)$ is the closed loop transfer $w \to y_1$ obtained from plant P, $\widetilde{T}_{ze}(K)$ refers to the transfer $e \to z$ in plant $\widetilde{P}$, and the channel $w \to z_u$ in plant P is a safeguard against unrealistic control actions. This leads to satisfactory results in the blue case, even though the stability certificate is weaker in the sense that the non-linear closed loop trajectory $x_{cl}(t)$ is only guaranteed locally exponentially stable and globally bounded.

Remark 6. The peak-gain or peak-to-peak norm $\|\cdot\|_{\mathrm{pk\_gn}}$ is the time domain L_∞-operator norm, which for SISO systems equals the time-domain L_1-norm of the impulse response, or the total variation of the step response [16, Sect. 5.2]. It is harder to compute, let alone to optimize, than the H_∞-norm, but the bound $\|H\|_\infty \le \|H\|_{\mathrm{pk\_gn}}$ is known. Non-smooth analysis of $\|\cdot\|_{\mathrm{pk\_gn}}$ is beyond the scope of this work and will be presented elsewhere. In our experiments we use the trapezoidal rule to estimate the integral of the absolute value of the impulse response of $(\widetilde{P}, K)$, and a heuristic to optimize it. Bounds for $\|\cdot\|_{\mathrm{pk\_gn}}$ have been discussed e.g. in [10], and a minimization approach via linear programming is discussed in [19] for the case of full order (unstructured) K.

7. Experiments

7.1. **Gray scenario.** The gray scenario has been addressed with the approach (29), where $q_l = -4.8$, $q_u = -4.8$, $W_u = \frac{1\mathrm{e}4s}{s+2\mathrm{e}5}$. Using Kalman reduction to determine a minimal realization, the finite-difference model with $N = 50$ is used to design a preliminary controller $K_0 \in \mathscr{K}_5$ in the class of 5^{th}-order controllers. The Nyquist test [5, Thm. 1] and Corollary 2 show that K_0 already stabilizes the linear infinite dimensional loop exponentially. Moreover, K_0 satisfies the sector constraint $\|\widetilde{T}_{ze}(K_0)\|_\infty = 0.281 < r^{-1} = 1/2.64 = 0.379$ strictly. After choosing a small enough tolerance with $\|\widetilde{T}_{ze}(K)\|_\infty + \vartheta < r^{-1}$, we check using [5, Thm. 2] that K_0 satisfies even the infinite dimensional sector constraint, so that the non-linear closed loop (G_{nl}, K_0) is *proved* globally exponentially stable in the sense of Proposition 3.

In a second phase this controller is further optimized with the true infinite dimensional system as described in [5], maintaining the stability and performance certificates already achieved during optimization. Ultimately this leads to the controller $K_{\text{gray}} \in \mathscr{K}_5$ in (31) which has the same stability certificates, and slightly improved H_∞-performance. This controller was then tested in non-linear simulations with spatial discretizations $N = 200$. For instance, in Fig. 10 (left) an initial condition $\theta_t(0) < \theta_t^0 = \Omega$ representing a deviation of 60% from the steady-state was chosen. The controller was switched on at time $t = 10$ and simulated with a square-wave disturbance occurring at $t = 15$ with magnitude 60% of the steady-state. In the gray scenario linear and non-linear trajectories are almost identical. That slip-stick may still occur even for this highly stable scenario is seen in Fig. 8 (right), but due to stability the trajectory θ_t is able to free herself and regain speed.

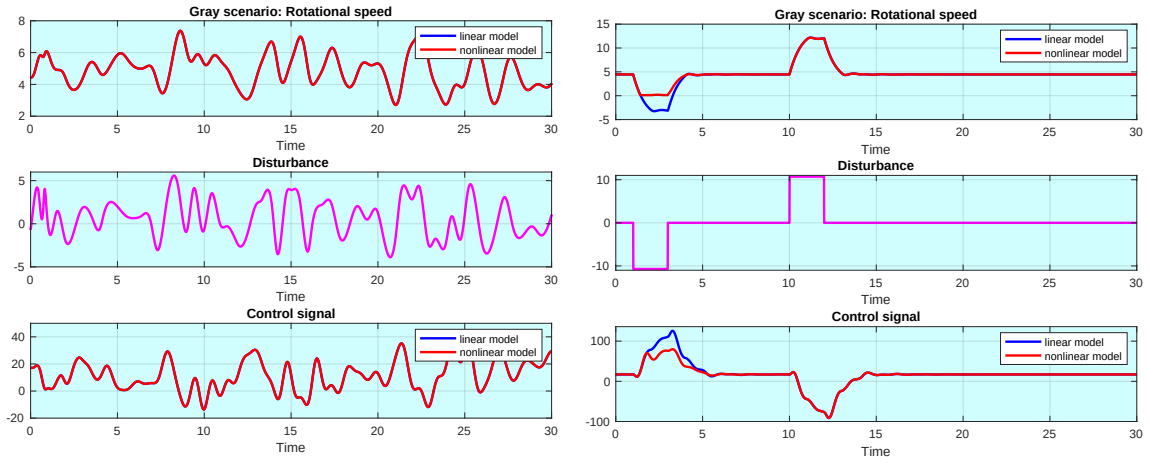

FIGURE 8. Gray scenario: Occasional slip-stick occurs even with global stability. Oscillatory disturbance (left). Disturbance at $t = 3, 10$ (right).

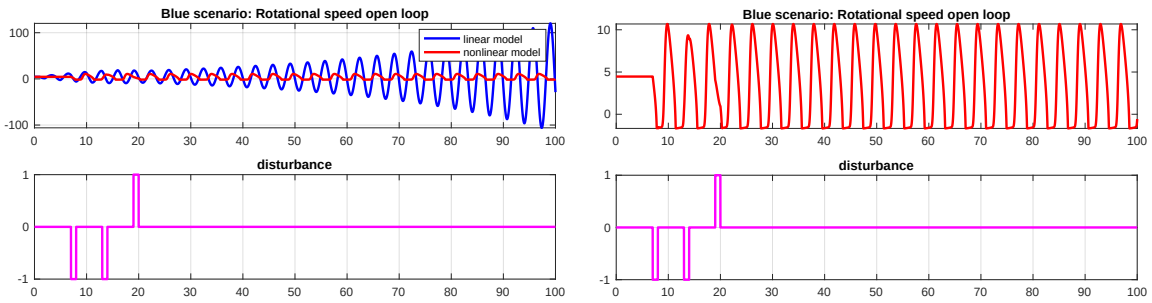

FIGURE 9. Blue scenario: Slip-stick in open loop.

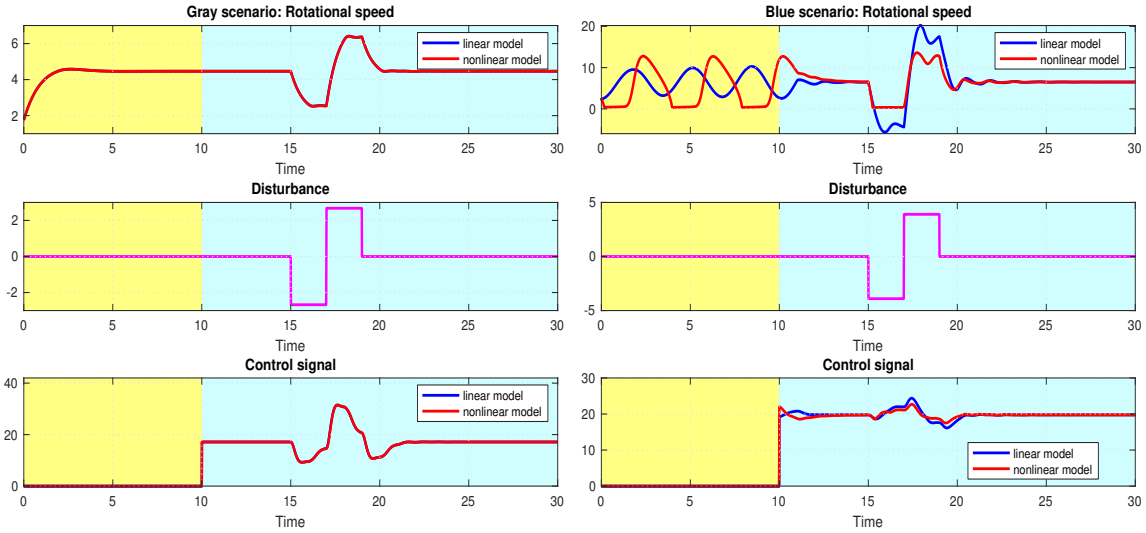

FIGURE 10. Initial value below steady state, control switched on at $t = 10$. Disturbance at $t = 15$. Gray left, blue right.

(31)

$$K_{\text{gray}} = \left[\begin{array}{c|c} A_K & B_K \\ \hline C_K & D_K \end{array}\right] = \left[\begin{array}{ccccc|cc} -0.80046 & -7.7472 & 0 & 0 & 0 & -13.0415 & 11.9996 \\ -1.9826 & -16.5346 & 41.59 & 0 & 0 & -25.1033 & 11.7281 \\ 0 & -1.103 & -2.6164 & 14.2226 & 0 & -12.39 & 0.012639 \\ 0 & 0 & -2.5597 & -2.6421 & 6.1304 & 2.1379 & 0.89566 \\ 0 & 0 & 0 & 3.2099 & -174.8766 & 0.90446 & -2.2903 \\ \hline 0.044385 & 0.23863 & -1.6385 & 0.48079 & 2.0247 & -2.0699\text{e}{-5} & 5.7173\text{e}{-6} \end{array}\right]$$

$$K_{\text{blue}} = \left[\begin{array}{c|c} A_K & B_K \\ \hline C_K & D_K \end{array}\right] = \left[\begin{array}{ccccc|cc} -0.61907 & -1.1401 & 0 & 0 & 0 & 0.25637 & 0.17058 \\ 16.7706 & -4.1928 & -1.523 & 0 & 0 & -1.2753 & 0.43077 \\ 0 & 8.1615 & -6.3251 & -1.5961 & 0 & -0.40252 & -0.56916 \\ 0 & 0 & -1.7351 & -27.1582 & -4.1308 & -1.3393 & 5.0511 \\ 0 & 0 & 0 & -17.2811 & -83.1511 & 5.0909 & 3.4138 \\ \hline -11.1263 & 3.7925 & -1.4411 & -2.7711 & 3.9251 & -9.9964\text{e}{-5} & -2.355\text{e}{-6} \end{array}\right]$$

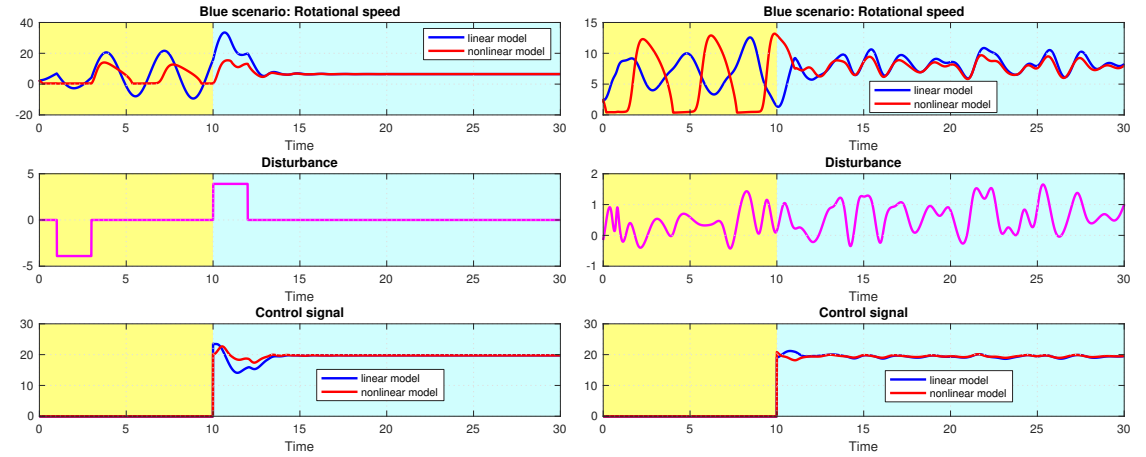

FIGURE 11. Blue scenario: slip-stick caused by large disturbances. Stabilizing feedback with K_{blue} allows the rotational speed to recover.

7.2. **Blue scenario.** The blue scenario is more challenging as the damping parameter λ is between the two critical values $\lambda_1(\alpha, q) < \lambda < \lambda_2(\alpha, q)$, giving rise to two unstable poles. Here slip-stick occurs quickly in open loop (Fig. 9). While stabilization of the linear closed loop is based on the results of section 5, leading to a locally exponentially

stable non-linear closed loop, a global certificate via the sector non-linearity (29) fails due to the very large primal sector in the blue case. In response, we use the large magnitude sector constraint in tandem with overshoot mitigation. Moreover, the H_2-norm is used as a heuristic for the peak-gain norm, which leads to the mixed program

$$\begin{array}{ll} \text{minimize} & \|T_{y_1 w}(K)\|_\infty \\ \text{subject to} & \|\widetilde{T}_{ze}(K)\|_2 \le \rho(r) \\ & \|W_u T_{uw}(K)\|_\infty \le 1 \\ & K \in \mathscr{K}_5, \end{array} \tag{32}$$

the parameters now being $q_l = -3$, $q_u = -0.1$ and $W_u(s) = \frac{1e4s}{s+2e5}$.

The idea is to employ the H_2-norm of the LTI-system in Fig. 7 as an indirect means to reduce $\|\widetilde{T}_{ze}(K)\|_{\mathrm{pk\_gn}}$, which amounts to replacing the L_1-norm of the impulse response by its energy. The parameter $\rho(r)$ has been estimated using trial and error so that the H_2 constraint ensures satisfaction of the peak-gain constraint in program (30) with parameter r. Starting again with $K_0 \in \mathscr{K}_5$ synthesized for a finite-difference model with $N = 50$, we certify exponential stability and H_∞-performance of the infinite-dimensional loops (P, K_0) and $(\widetilde{P}, K_0)$ via [5], and the H_2-certificate with [4, Lemma 3]. This controller is further optimized in the true infinite dimensional system using the method of [5, 4], leading to the final $K_{\mathrm{blue}} \in \mathscr{K}_5$ in (31). We recall that Corollary 2 in tandem with the Nyquist test of [5] proves that K_{blue} stabilizes (1)-(2) locally exponentially, its linearization exponentially, while [5, Thm. 3] certifies the H_∞-norm estimates in (32). Posterior certification of the H_2-norm estimate in (32) is also possible, now via [4], and proves $\|\widetilde{T}_{ze}(K_{\mathrm{blue}})\|_2 < \rho(r) = 1.3$ in the infinite-dimensional sense. Due to the choice of $\rho(r)$ this now implies $\|\widetilde{T}_{ze}(K_{\mathrm{blue}})\|_{\mathrm{pk\_gn}} = 0.680 < r^{-1} = 1/1.45 = 0.690$, whereby the complementary large magnitude sector condition is verified in the discretized model with $N = 200$. Infinite dimensional certification for $\|\cdot\|_{\mathrm{pk\_gn}}$ is currently not yet available, even though this ought to be established along the lines of [5, Lemma 4, Theorem 3] and [4, Lemma 3]. The controller achieves excellent results in the non-linear simulation. This is shown in Fig. 10 (right), where an initial condition generates slip-stick in open loop (yellow area). Triggering control at $t = 10$ removes slip-stick and additionally provides rejection against strong and sharp disturbances (blue area). Similarly, in Fig. 11 the effect of switching the controller on at $t = 10$ is tested on two more disturbances.

It should be mentioned that other ways to address the non-linearity ψ have been discussed. In [17] an adaptive controller for a time varying $q(t)$ was constructed, while [4] discusses parametric robust control for $q \in [\underline{q}, \overline{q}]$ as well as gain-scheduling of $q(t)$ as further possibilities.

Conclusion

We have presented a novel method to design exponentially stabilizing regulators of simple implementable structure for boundary control of a wave equation with non-linear boundary anti-damping. Our results are illustrated in control of torsional vibrations in drilling systems, and two scenarios labeled 'gray' and 'blue' are discussed in detail. We show that in order to avoid slip-stick it is crucial to optimize H_∞-performance of the loop. In particular, reducing overshoot by way of H_∞ minimization proved effective for the more challenging 'blue' scenario. The 'gray' scenario had previously been discussed in the literature, and here the substantial improvement of our method over published work is that we can design finite-dimensional exponentially stabilizing controllers, which in addition show excellent performance. The 'blue' scenario is new and more challenging due to inherent instability. We design finite-dimensional controllers which stabilize the

wave equation locally exponentially, mitigate the slip-stick effect, and in addition, have a global boundedness certificate, based on the novel concept of a large magnitude sector non-linearity.

References

[1] U.J.F. Aarsnes, D. Di Meglio, R.J. Shor. Avoiding stick slip vibrations in drilling through startup trajectory design. *Journal of Process Control* 70:2018,24-35.

[2] A.M. Annaswamy, A.F. Ghoniem. Active control of combustion instability: Theory and practice. *Control Systems, IEEE*, 22(6):2002,37-54.

[3] P. Apkarian, M. N. Dao, D. Noll. Parametric robust structured control design, *IEEE Transactions on Automatic Control* 60 (7):2015,1857–1869.

[4] P. Apkarian, D. Noll. Boundary control of partial differential equations using frequency domain optimization techniques. *Systems and Control Letters*, to appear.

[5] P. Apkarian, D. Noll. Structured H_∞-control of infinite dimensional systems, *Int. J. Robust Nonlin. Control* 28(9):2018,3212–3238.

[6] P. Apkarian, D. Noll. Nonsmooth H_∞ synthesis, *IEEE Trans. Automat. Control* 51 (1) (2006) 71–86 (January 2006).

[7] P. Apkarian, D. Noll. Nonsmooth optimization for multidisk H_∞ synthesis, *European J. of Control* 12 (3):2006,229–244.

[8] P. Apkarian, D. Noll, L. Ravanbod. Nonsmooth bundle trust-region algorithm with applications to robust stability, *Set-Valued and Variational Analysis* 24 (1):2016,115–148.

[9] P. Apkarian, D. Noll, L. Ravanbod. Non-smooth optimization for robust control of infinite-dimensional systems, *Set-Valued Var. Anal.* 26(2):2018,405-429.

[10] V. Balakrishnan, S. Boyd. On computing the worst case peak gain of linear systems. *Systems and Control Letters* 19(4):1992,265-269.

[11] M. Barreau, F. Gouaisbaut, A. Seuret. Stabilization of an unstable wave equation using an infinite dimensional dynamic controller. *57th IEEE Conf. on Dec. Control (CDC), 2018, Miami Beach.* `10.1109/CDC.2018.8619356`.

[12] M. Barreau, A. Seuret, F. Gouaisbaut, L. Baudouin. Lyapunov stability analysis of a string equation coupled with an ordinary differential system. *IEEE Trans. Automatic Control*, 2018.

[13] H.I. Basturk. Observer-based boundary control design for the suppression of slip-stick oscillations in drilling systems with only surface measurements. *J. Dynamic Syst., Measurement, and Control*, 139:2017, 104501-1.

[14] L. Beji, L. Benchikh. A method of drilling a ground using a robotic arm. *Int. J. Mech. Mechat. Eng.* 11(11):2017,1821-1826.

[15] B. Besselink, T. Vromen, N. Kremers, N. van de Wouw. Analysis and control of stick-slip oscillations in drilling systems. *IEEE Trans. Control. Syst. Tech.* 24(5):2016,1582-1593.

[16] S.P. Boyd, C.H. Barratt. *Linear controller design. Limits of performance.* Prentice Hall 1991.

[17] D. Bresch-Pietri, M. Krstic. Output-feedback adaptive control of a wave PDE with boundary anti-damping, *Automatica* 50 (5):2014,1407–1415.

[18] N. Challamel. Rock destruction effect on the stability of a drilling structure. *Journal of Sound and Vibration* 233:2000,235-254.

[19] I.J. Diaz-Bobillo, M.A. Dahleh. Minimization of the maximum peak-to-peak gain: the general multi-block problem. *IEEE Transactions on Autom. Contr.* 38(10):1993,1459-1482.

[20] A. Cheng, K. Morris. Well-posedness of boundary control systems. *SIAM J. Control Optim.* 42(4):2003,1244-1265.

[21] J. Cheng, M. Wu, C. Lu, L. Chen, X. Chen, W. Cao, X. Lai. A stick-slip vibration suppression method for the drillstring system based on neutral type model. *11th Asian Control Conf. (ASCC), Australia, 2017.*

[22] R. F. Curtain, H. Zwart. *An Introduction to Infinite-Dimensional Linear Systems Theory.* Vol. 21 of Texts in Applied Mathematics, Springer-Verlag, 1995 (1995).

[23] M.A. Davó, D. Bresch-Pietri, C. Prieur, F. Di Meglio. Stability analysis of a 2×2 linear hyperbolic system with a sampled-data controller via backstepping method and looped-functionals. *IEEE Trans. Autom. Contr.* to appear.

[24] E. Fridman, S. Mondié, B. Saldivar. Bounds on the response of a drilling pipe model. *Special issue on Time-Delay Systems in: IMA Journal of Mathematical Control & Information*, 27:2010, 513-526.

[25] Hsiao-Ping Huang, Chung-Tarng Jiang, and Yung-Chen Chao. A new Nyquist test for the stability of control systems. *International Journal of Control* 58(1):97–112, 1993.
[26] K. Morris. Justification of input-output methods for systems with unbounded control and observation, *IEEE Trans. Autom. Control* 44 (1):1999,81–85.
[27] E. Navarro-Lopéz, D. Cortés. Avoiding harmful oscillations in a drillstring through dynamical analysis. *Journal of Sound and Vibration,* 307:2007, 152-171.
[28] D. Noll. Bundle method for non-convex minimization with inexact subgradients and function values, Computational and Analytical Mathematics. *Springer Proceedings in Mathematics & Statistics* 50 (2013) 555–592 (2013).
[29] K.-J. Engel, R. Nagel. *One-Parameter Semigroups for Linear Evolution Equations.* Springer Graduate Texts in Mathematics, Springer Verlag, 2000.
[30] I.M.Y. Mareels, D.J. Hill. Monotone stability of non-linear feedback systems. *J. Math. Syst., Est. and Control* 2(2):1992,275-291.
[31] D. Mugnolo. Damped wave equations with dynamic boundary conditions. *J. Appl. Anal.* 17(2):2011,241-275.
[32] D. Pilbauer, D. Bresch-Pietri, F. Meglio, C. Prieur, T. Vyhlídal. Input shaping for infinite dimensional systems with application on oil well drilling. *16th European Control Conference (ECC 2018), June 2018, Limassol, Cyprus.*
[33] C. Roman, D. Bresch-Pietri, C. Prieur, O. Sename. Robustness to in-domain viscous damping of a collocated boundary adaptive feedback law for an anti-damped boundary wave PDE. *IEEE Trans. Autom. Control* 64(8):2019,3284-3299.
[34] C. Roman, D. Bresch-Pietri, E. Cerpa, C. Prieur, O. Sename. Backstepping control of a wave PDE with unstable source terms and dynamic boundary. *IEEE Contr. Syst. Letters* 2(3):2018,459-464.
[35] C. Sagert, F. Di Meglio, M. Kristic, P. Rouchon. Backstepping and flatness approaches for stabilization of the slip-stick phenomenon for drilling. *IFAC Proc. Volumes* 46(2):2013,779-784.
[36] D. Salamon, Infinite dimensional linear systems with unbounded control and observation: a functional analytic approach, *Transactions of the American Mathematical Society* 300 (2) (1987) 383–431 (1987).
[37] D. Salamon, Realization theory in Hilbert space. *Math. Syst. Theory* 21:1989,147-164.
[38] B. Saldivar, S. Mondié, J.-J. Loiseau. Reducing stick-slip oscillations in oil-well drillstrings. *6th Int. Conf. Elect. Eng., Comp. Sci. Autom. Control (CCE)*, Toluca, Mexico, 2006.
[39] B. Saldivar, S. Mondié, J. Loiseau, V. Rasvan. Suppressing axial-torsional vibrations in drillstrings. *Journal of Control Engineering and Applied Informatics,* SRAIT, 14:2013,3-10.
[40] B. Saldivar, S. Mondié, J.C. Ávila Vilchis. The control of drilling vibrations: a coupled PDE-ODE modeling approach. *Int. J. Appl. Math. Comp. Sci.* 26(2):2016,335-349.
[41] B. Saldivar Márquez, I. Boussaada, H. Mounier, S.-I. Niculescu. *Analysis and Control of oil-well Drilling Vibrations.* A Time-Delay System Approach. Springer Series Advances in Industrial Control, 2015.
[42] A.F.A. Serrarens, M.J.G. van de Molengraft, J.J. Kok, L. van den Steen. H_∞ control for suppressing stick-slip in oil well drillings. *IEEE Control Systems*, 18(2):1998,19-30.
[43] A. Smyshlyaev, B.-Z. Guo, M. Krstic. Arbitrary decay rate for Euler-Bernoulli beam by backstepping boundary feedback. *IEE Trans. Autom. Contr.* 54(5):2009,1134-1140.
[44] A. Smyshlyaev, M. Krstic. Boundary control of an anti-stable wave equation with anti-damping on the uncontrolled boundary, *Systems and Control Letters* 58:2009,617-623.
[45] O. Staffans. *Well-Posed Linear Systems*, Encyclopedia of Mathematics and its Applications, Cambridge University Press, 2005.
[46] S. P. Timoshenko. *Vibrations Problems Engineering.* Princeton, NJ: D. Van Nostrand Company, 1955.
[47] R. Tucker, C. Wang. In integrated model for drill-string dynamics. *Journal of Sound and Vibration*, 224, 1999,123-165.
[48] R. Tucker, C. Wang. Torsional vibration control and cosserat dynamics of a drill-rig assembly. *Mecanica*, 33, 2003, 145-161.
[49] G. Weiss, R. Rebarber. Dynamic stabilizability of well-posed linear systems. *5th International Symposium on Methods and Models in Automation and Robotics*, Miedzyzdroje, Poland, 1:2-9, 1998.
[50] G. Zames. On the input-output stability of time-varying non-linear feedback systems. Part I: Conditions derived using concepts of loop gain, conicity, and positivity. *IEEE Trans. Autom. Control*, AC-11(2):1966,228-238.

[51] G. Zames, P.L. Falb. Stability conditions for systems with monotone and slope-restricted nonlinearities. *SIAM J. Control* 6(1):1968,89-108.
[52] K. Zhou, J.C. Doyle, K. Glover. *Robust and Optimal Control*. Prentice Hall 1996.
[53] H. Zwart. Linearization and exponential stability. arXiv:1404.3475v1, 2014.
[54] Robust Control Toolbox 5.0, MathWorks, Natick, MA, 2013 (2013).